Nonlinear Line-Element Modeling of Flexural Reinforced Concrete Walls

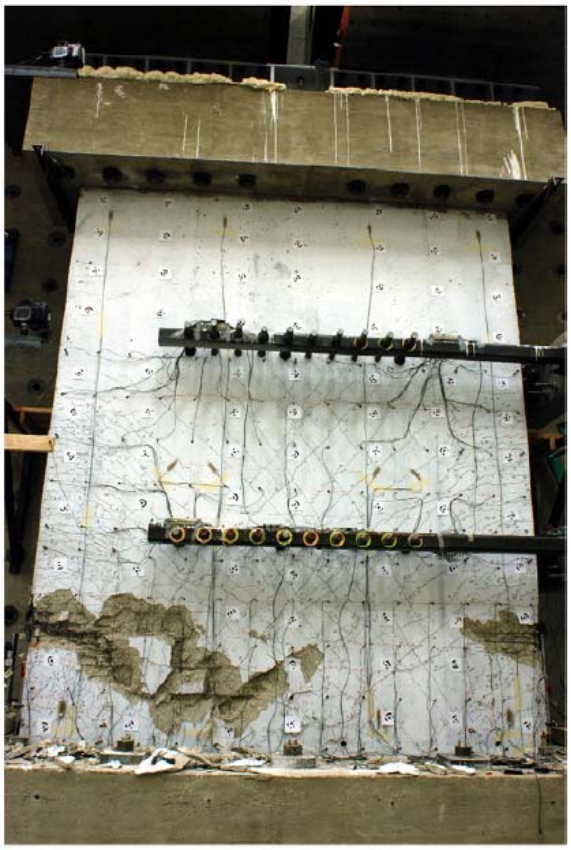

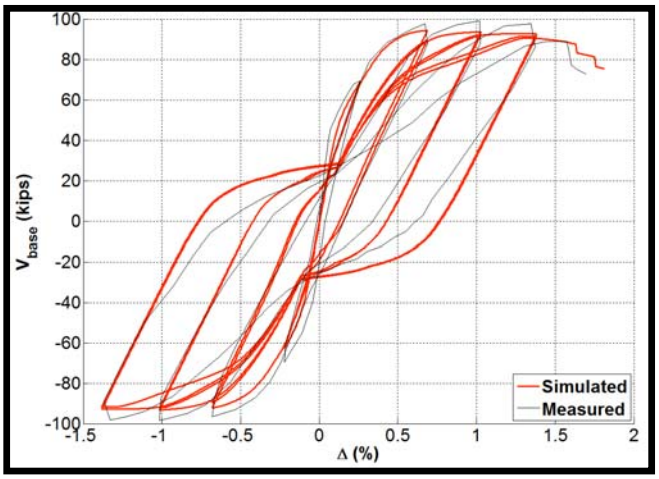

Dr. Joshua Pugh, EDG Inc.
Dr. Laura Lowes, University of Washington
Dr. Dawn Lehman, University of Washington

Funding provided by the **National Science Foundation** and the **Charles Pankow Foundation**

CHARLES PANKOW
FOUNDATION

Nonlinear Line-Element Modeling of Flexural Reinforced Concrete Walls

Joshua S. Pugh, EDG Inc., Laura N. Lowes and Dawn E. Lehman, University of Washington

ABSTRACT

Structural walls are commonly used as the lateral-load resisting system in high seismicity regions in the US. Although walls in low-rise construction are typically squat, slender walls with height to in-plan length ratios greater than two are typical in high and mid-rise construction; the response of these walls tends to be dominated by flexure. Simulation of the nonlinear earthquake response of a high- or mid-rise walled building requires a model that accurately captures flexural response in a computationally efficient manner. The research presented here developed a model to meet the dual objectives of accuracy and computational efficiency. A review of experimental tests of concrete walls shows that walls with shear-span ratios greater than 2.0 and shear demand-capacity ratios less than 1.0 typically respond in flexure. However, even when designed to meet codified provisions for tension-controlled response, the most common failure mode for these walls is compression, which includes crushing of core concrete and bar buckling. The predominance of this failure mode is confirmed by post-earthquake reconnaissance. Less common is a true tension-controlled failure, with direct or low-cycle fatigue induced fracture of the bars. Therefore, nonlinear wall models must be capable of simulating strength loss due to compression failure. To investigate the accuracy of common modeling approaches and to advance these approaches as required, a research program was undertaken. First, the experimental database was developed and modeling approaches (e.g., lumped plasticity, distributed plasticity, and continuum elements) were reviewed. The evaluation indicated that the most viable option to achieve accuracy and efficiency was the use of beam-column line elements with fiber-type cross-section models at the integration points. Initially, both displacement-based and force-based element formulations were evaluated; however, the displacement-based formulation resulted in an inaccurate representation of the axial force distribution along the length of the element. Therefore, only the force-based formulation was chosen for further study. The basic model included standard 1D constitutive models for confined concrete, plain concrete and reinforcing steel. Comparing simulated and measured response data showed that the concrete and steel material models must be regularized using a mesh-dependent characteristic length and a material-dependent post-yield energy to enable accurate, mesh-objective simulation of strength loss due to compression failure. The post-yield energy values were determined using relevant experimental data, an important but missing component of prior research on material regularization. The results of this study show that use of the regularized constitutive models results in accurate simulation of response for planar walls subjected to unidirectional loading and for c-shaped walls subjected to unidirectional and bidirectional loading. Accurate simulation of response is not achieved for t-shaped walls. This is attributed to the simplifying assumptions of a linear axial strain field across the member cross section and decoupling of flexure-shear response, both of which are particularly erroneous for t-shaped walls.

INTRODUCTION

Reinforced concrete walls are used commonly in mid- and high-rise buildings to resist earthquake loads. As such, numerical models are required that provide accurate prediction of the response of these walls under earthquake loading, including accurate prediction of the stiffness, strength, drift capacity and hysteretic response. Engineers require these models to enable performance-based design of walled buildings, and researchers require these models to investigate the behavior and performance of walls as well as to advance seismic design procedures for walls.

The primary objective of the research present herein was to develop practical recommendations for modeling slender walls, which respond primarily in flexure. Computationally efficient beam-column elements were selected; these elements are readily available in nonlinear structural analysis software packages. Therefore a secondary objective was to identify the domain for which these models provide accurate prediction of response.

Performance-based earthquake engineering requires accurate assessment of all aspects of the response, including strength degradation. To better understand the response and failure mode of flexural walls, a brief review of experimental investigation of wall behavior is provided. The review indicates that response models for slender walls must be capable of simulating tension, compression, and shear responses as well as compression and tension failure modes. Commonly used elements for wall modeling are reviewed with an emphasis on line elements, which can provide computationally efficient simulation of response. Current line-element formulations use conventional 1D constitutive models for concrete and reinforcing steel and fiber-type section models; these models are used for commonly for reinforced concrete beams and columns. These conventional approaches are evaluated using data from 21 slender planar wall tests. The results show that for walls exhibiting compression-controlled response, conventional models fail to converge to a single solution. An alternative approach is developed using regularized constitutive models. The proposed modeling approach is compared with experimental results to proposed methodology for nonlinear simulation of slender walls.

Experimental Behavior of Slender Concrete Walls

Experimental testing indicates that slender walls with shear-span ratios (distance between the heights at which the wall has zero and maximum moment divided by the length of the wall) greater than 2.0 typically respond in flexure (Pugh 2012). Walls with shear-span ratios exceeding 2.0 are common and therefore accurate modeling of their response, including strength degradation, is needed for seismic design and assessment of buildings that have structural walls as their primary lateral load system.

As part of a companion research effort, Birely (2012) evaluated over 60 slender (shear-span ratio greater than 2.0) experimental wall specimens. Study of the tests indicated that failure, i.e. degradation in the lateral load carrying capacity, of a flexural wall is a result of one or more damage modes: (1) compression damage which includes crushing of boundary-element concrete and buckling of boundary element reinforcing steel (Figure 1a), (2) low-cycle fatigue of the reinforcement, which includes buckling and subsequent fracture of longitudinal steel, and (3) rupture of longitudinal steel (Figure 1b). For some walls, the primary failure mode is shear; data analysis suggests that this mode is exhibited for high shear demands in particular if the ratio of the shear demand (V_u) to ACI (ACI 318 2011) capacity (V_n) exceeds 1. Figure 2 shows the observed damage modes of the slender-wall database. As indicated in the plot, the majority of the walls exhibited a compression-controlled failure mode (i.e., boundary element crushing). It is of note that all of the walls that exhibited compression-controlled failure satisfied the ACI tension-controlled design limit (ACI 318 2011). Therefore, simply designing a wall to meet the tension-control criterion does not necessarily result in tension-controlled failure.

Although slender walls may not exhibit typical shear damage (e.g., diagonal cracking or crushing along a diagonal line), experimental research indicates that the impact of shear on wall response is not negligible. For example, consider experimental tests on well-confined planar walls by Lowes et al. (2012). In this study, two of the tests were designed to be nominally identical with different level of shear demand (the plastic shear demand was increased by decreasing the moment applied to the top of the specimen and thereby decreasing the effective height). Although neither specimen exhibited a shear failure mode, the specimen with the higher shear demand had a lower drift capacity. Additionally, these

flexural walls sustained shearing deformations that accounted for as much as 30% of total wall deformation (Lowes et al. 2012). Both results indicate that including shear in wall models is important.

Prior Research Studies on Simulation of Walls

There are a wide range of modeling approaches that have been used to simulate the behavior of concrete walls. In engineering practice, it is typical to model part or all of the building structure; therefore, computationally efficient models are typically used. Most nonlinear analysis software used in the design office includes line elements. Within the category of line-element models, a range of formulations exist including concentrated hinge models, fiber-section lumped plasticity models and distributed plasticity beam-column elements. Research efforts have also studied the use of line-element models, as described below. However few programs have conducted a systematic evaluation of this approach using a substantial experimental database, and therefore it is difficult to determine their accuracy solely using the results of prior research.

Other researchers have used continuum models to simulate walls. This category of modeling typically includes shell elements, fiber shell elements, and solid elements. These models are advantageous in that nonlinear shear response and flexure-shear interaction are captured by the model. However, continuum modeling approaches are computationally expensive and therefore are not commonly used in practice. Some of the relevant research using both line-element and continuum-element models are summarized below. Additional information may be found in Pugh (2012).

One of the simplest and most basic approaches to simulating the nonlinear response of walls is to use a lumped-plasticity line-element model. The lumped-plasticity model locates a flexural hinge at the critical section with an elastic beam-column element used to model the remainder of the wall. Since the concrete and steel materials are not modeled explicitly, a multi-linear moment-rotation response curve is used. The only standardized curve for walls is specified in ASCE 41 Supplement 1 (2007). ASCE 41 provides a backbone curve; model parameters for the cyclic response are not provided. The parameters of the backbone curve depend on the axial load ratio, shear stress demand and confinement. Although the approach is computationally efficient, its accuracy is limited to the calibrated parameter values. In addition, the moment-rotation response of the hinge must be defined prior to the analysis; therefore the model cannot account for the impact on response of variation in axial or shear load. If hinging occurs away from the assumed critical section, multiple analyses are required in which additional hinges are introduced. Research indicates that the current ASCE 41 parameters may underestimate the strength and deformability of more slender walls (Massone 2006). Because of its simplicity, computational efficiency and robustness, this modeling approach is used commonly in practice and to investigate the seismic response and design of walled buildings (Panneton et al. 2006, Calugaru and Panagiotou 2012, Rejec et al. 2012).

More sophisticated lumped-plasticity models simulate the flexural response of the wall cross section using a fiber-type discretization model. This approach permits computation of the moment-curvature response of the critical section; a plastic-hinge length is commonly used to compute the moment-rotation response. The fiber discretization of the section comprises concrete and steel “fibers” for which stress-strain response is defined by one-dimensional constitutive models. The curvature and average axial strain imposed on the section determine the axial strain of the individual fibers; the moment and axial loads are computed from the fiber stresses and areas. This type of lumped-plasticity model simulates the impact of axial load on flexural response. The cyclic response of the section and component are also modeled directly if cyclic material constitutive models are employed. There are disadvantages to this modeling approach. These models employ the assumption of a linear strain field,

which may introduce error for some wall configurations (e.g. long planar walls and walls with long flanges). Flexure-shear interaction is also neglected. Finally, the value and static nature of the plastic hinge length may introduce errors. As discussed above, multiple analyses with updated models may be required to accurately simulate the distribution of nonlinearity along the wall height. Although a viable approach, no studies were found in the literature validating it for wall modeling.

An alternative to the lumped-plasticity element is the distributed-plasticity beam-column element. Typically, a fiber cross section is incorporated into these elements. Displacement-based and force-based distributed-plasticity beam-column element formulations exist in the literature (e.g. Zeris and Mahin 1988, Spacone et al. 1996, Scott and Fenves 2006). Displacement-based elements employ the assumptions of a linear curvature field and constant average axial deformation field along the length of the element. Force-based elements employ the assumptions of a linear moment and constant axial force distributions along the length of the element. Because these elements are used with a displacement-based finite element analysis, in which compatibility between elements is satisfied apriori and nodal displacements are determined to satisfy nodal equilibrium, the use of force-based elements requires an intra-element solution to determine the element force distribution that produces the nodal displacements that satisfy compatibility between elements.

Distributed-plasticity elements include multiple nonlinear fiber-type sections along the length of the element. This enables explicit simulation of nonlinear action at multiple locations up the height of the wall, overcoming a significant shortcoming of lumped-plasticity models. Some of the limitations noted with the fiber cross-section lumped-plasticity element are shared by the distributed-plasticity elements including i) the assumption of a linear strain field across the section and ii) the decoupling of flexure and shear response. Additionally, a relatively fine mesh of displacement-based elements may be required to accurately simulate response at locations up the height of the wall where inelastic action is significant, and force-based elements may exhibit convergence problems when strength degradation occurs. However, these models are computationally efficient, typically numerically robust, and represent a potentially powerful tool for nonlinear analysis of walled buildings. Boivin and Paultre (2012) employ a fiber-section model and the distributed-plasticity force-based beam-column element implemented in OpenSees to investigate shear and moment demands in slender walls subjected to earthquake loading.

A number of variations on the fiber-section hinge model and the fiber-section distributed-plasticity beam-column element have also been employed and implemented in research and commercial software to simulate wall response. For example, Orakcal et al. (2004) employ the multiple-vertical-line-element model (MVLEM) proposed by Vulcano et al. (1988) to simulate the nonlinear flexural response of slender walls. The MVLEM is essentially a finite-length fiber-section model combined with a horizontal spring that simulates the shear flexibility of the wall; Orakcal et al. employ standard one-dimensional cyclic constitutive models to define the response of concrete and steel fibers and an elastic shear-response model. Orakcal and Wallace (2006) show that the MVLEM can provide accurate simulation of wall response for walls for which the assumptions of plane sections remain plane, elastic shear response, and decoupling of flexure and shear response are valid. Ghobarah et al. (2004) and Galal (2007) simulated the response of a five-story wall subjected to dynamic shake-table loading (CAE 2002) using a model in which fiber-type sections were placed between elastic two-dimensional plane-stress elements (a plane-sections-remain-plane constraint was imposed at the interface between the fiber-section and the plane-stress elements); the model provided reasonably accurate simulation of strength and hysteretic response under dynamic loading. Finally, the fiber shell wall element implemented in Perform (http://www.csi.berkeley.edu) may be considered a variation of the fiber-type section model as

flexural response is determined by the stress-strain response of vertical fibers with shear response determined by an independent one-dimensional shear model.

Multiple researchers have sought to improve simulation of walls using fiber-section distributed-plasticity elements by incorporating simulation of flexure-shear interaction. In these models, fiber response is typically defined by a two-dimensional strain field, the assumption that fibers are in a state of plane stress, and a two-dimensional constitutive model. Examples of this type of model include that proposed by Jiang and Kurama (2010) and by Petrangeli et al. (1999), both of which use the "microplane" model (Bazant and Oh 1985, Bazant and Prat 1988; Bazant and Ozbolt 1990; Ozbolt and Bazant 1992) to define multi-dimensional concrete response. Response 2000 (Bentz 2000) employs a similar approach with multi-dimensional concrete response defined using the Modified Compression Field Theory (Vecchio and Collins 1986). Jiang and Kurama (2010) show that this modeling approach enables simulation of nonlinear shear response, interaction of flexure and shear mechanism and reasonably accurate simulation of observed response for a limit number of wall specimens. However, while these models provide the potential for improved simulation of response, the flexure-shear fiber-section elements are more computationally demanding and less numerically robust than the models in which flexure and shear response are decoupled. Additionally, these models are limited by the assumption about the shear strain distribution on the section. Finally, this approach is limited by the difficulty of using line elements to model complex wall geometries.

Analysis using continuum elements (i.e. shell and solid elements) has the potential to provide more accurate simulation of nonlinear wall response than the models discussed above. Continuum models do not require simplifying assumptions about the strain or stress field at the section level, inherently simulate the interaction of nonlinear flexure, shear and torsional response modes, and facilitate representation of complex wall configurations (e.g., C, T, and H cross sections). For isolated planar and, in some cases, non-planar walls, two-dimensional plane-stress elements can provide accurate results. For non-planar walls, fiber shell elements (where fibers are two-dimensional and concrete fiber response is determined using a two-dimensional plane-stress concrete constitutive model) or three-dimensional brick elements can provide accurate simulation of response. The challenge with continuum analyses is that they are computationally demanding; this typically precludes their use in standard practice in particular when full building analyses subjected multiple ground motions are required. Additionally, implicit solution algorithms are typically used and are often plagued by convergence issues, especially when strength loss initiates. Research efforts have addressed the use of continuum elements. Palermo and Vecchio (2007) employed VecTor2 with two-dimensional plane stress elements and a variant of the two-dimensional modified compression field theory (MCFT) reinforced concrete constitutive model; satisfactory simulation of walls tested by Palermo and Vecchio (2002) was achieved. Others have used finite element analysis (FEA) programs (e.g., ATC 94 2012). Continuum-type models offer the potential for accurate simulation of both local response quantities and response mechanisms beyond flexure; however, the high computational demands associated with these models makes them impractical for use in practice or in research addressing the design and performance of structural systems.

The primary limitation of the prior studies is that a very limited data set was used to validate the models; typically the modeling approach was validated using data from 1 to 4 test specimens. The literature is rich with test data for structural walls, and a more thorough evaluation of wall models is warranted. The research presented herein evaluated commonly used line-element models using data for slender walls with a range of design characteristics tested using varying procedures and protocols. The

following sections describe the data set developed for the study and the evaluation procedure and results.

EVALUATION OF LINE ELEMENTS SEISMIC ANALSYIS OF WALLED BUILDINGS

Planar Wall Experimental Data Set

Previously tested slender planar (i.e. rectangular) wall specimens were used to evaluate the modeling approaches discussed above. The specimens were selected based on the following criteria:

- Planar (rectangular) wall specimen subjected to in-plane flexure, shear and axial loading.
- Specimen failure resulted from deteriorating flexural response. This included tension and compression controlled response (e.g., bar fracture or concrete crushing and bar buckling).
- Wall specimen thickness in excess of 76 mm (3 in.). Wall specimens thinner than this were not considered to exhibit behavior representative of full-scale reinforced concrete walls.
- Data required to fully define a numerical model were provided. Required data included concrete compressive strength (f'_c), defined reinforcing steel stress-strain response (f_y, f_u), specimen geometry, reinforcement layout, and test specimen boundary conditions in the laboratory.
- Data required to evaluate simulation results were provided. These included global load-displacement response and the observed failure mechanism.

The assembled data set included 21 reinforced concrete wall specimens from 7 experimental research programs (Table 1). Quantities in Table 1 are defined as follows:

- Aspect ratio = l_w/ where l_w = wall length and t = wall thickness
- Shear span ratio = $M/(Vl_w)$ where M is the moment developed at the base of the wall, V is the shear developed at the base of the wall and l_w is the planar length of the wall.
- Axial load ratio = $P/A_g f_c$ where P is the axial load at the base of the wall, A_g is the gross area of the wall and f_c is the concrete compressive strength.
- Shear stress demand = V_{max} / $A_{cv}(f_c)$^0.5 where V_{max} is the maximum base shear developed during the test, A_{cv} is the shear area, taken equal to $5/6A_g$ for a rectangular section, and f_c is the concrete compressive strength. Note that data are provided by f_c in MPa and psi
- Shear demand-capacity ratio = V_{max}/V_n where V_{max} is the maximum base shear and V_n is the shear strength computed per ACI 318 (2011) using actual concrete and steel strengths.
- Δ_y = drift capacity = drift at which the lateral load carrying capacity of the wall dropped to 80% of the historic maximum, for drift demands in excess of historic drift demands.
- Δ_u = drift capacity = drift at which the lateral load carrying capacity of the wall dropped to 80% of the historic maximum, for drift demands in excess of historic drift demands.

- Failure mode indicates the primary mechanism causing loss of lateral load carrying capacity: concrete crushing and buckling of longitudinal steel (CB), rupture of longitudinal steel (R) or buckling followed by rupture of longitudinal steel (BR).

A few important aspects of the database are of note. The aspect ratio of the walls was generally greater than 2.0 (two had ratios of 1.6) and the shear-demand capacity ratio was generally less than 1.0 (one has a ratio of 1.1). Both of these characteristics are expected for walls that exhibit a flexural response mode.

Nine (9) of the specimens sustained bar fracture; the remainder sustained a compressive failure mode. Most of the specimens were subjected to modest axial load ratios, with the largest axial load ratio being 0.13. While a compression-controlled failure is not commonly expected for a wall with a modest axial load, prior research by Birley (2012) and Pugh (2012) indicates that compression-controlled response is common for modern walls, even those designed to meet the tension-controlled flexural response criteria laid out in ACI 318-11. Figure 3 shows the tensile strain in the extreme reinforcing bar for specimens exhibiting the CB failure mode; for all of the specimens, tensile strains greatly exceed the ACI limit for tension-controlled flexure response, 0.005.

All of the specimens in the database were used to evaluate the basic and proposed modeling approaches. Detailed analysis results cannot be presented for each specimen due to length restrictions. Instead, results are tabulated where appropriate and a selected group of specimens are used to illustrate the results. Specifically four specimens were selected for presentation in the paper; these specimens span the range of failure modes identified above as well as a range of shear demands. Specimen WSH4 failed due to compression/buckling (CB). Specimen WSH1 failed due to bar rupture (R) and had a relatively low shear demand. Specimen RW1 failed due to bar buckling followed by bar rupture (BR). Specimen S6 failed due to compression/buckling (CB) and had a relatively large shear demand.

Non-Planar Wall Experimental Data Set

Modeling approaches were initially evaluated and modeling recommendations were ultimately developed using data from previous planar wall tests. The modeling recommendations developed as part of this study were then applied to simulate the response of non-planar walls subjected to unidirectional and bidirectional loading. Simulated and measure response histories were compared.

Non-planar wall specimens were selected for use in the study using the same criteria as were used to select planar wall specimens, with the exception that c-shaped and t-shaped wall specimens subjected to in-plane and/or out-of-plane flexure, shear and axial loading were considered. Table 2 lists design and response quantities for the non-planar wall data set, which includes 12 reinforced concrete wall specimens from 5 experimental research programs. Quantities in Table 2 are defined as in Table 1. In Table 2, Load Dir. indicates the direction of loading, where $\pm$X indicates lateral loading parallel to the web of the c-shaped wall or the flange of t-shaped walls. For loading in $\pm$X direction response is nominally symmetric in the positive and negative loading directions. Loading in the $+$Z or $-$Z indicates loading parallel to the flanges of the c-shaped walls or the web of the t-shaped wall; response is not symmetric. For c-shaped walls, $+$Z indicates loading putting the toes of the flanges in compression and the web of the wall in compression. For t-shaped walls, $+$Z indicates loading putting the toe of the web in compression and the flange of the wall in compression. For both t-shaped and c-shaped walls, loading in the $+$Z direction could be expected to result in greater strength than loading in the and $-$Z direction, assuming constant axial load.

THE BASIC MODEL

Fiber-type beam-column elements have distinct advantages for simulating the nonlinear response of reinforced concrete and steel structures in engineering practice. These types of models are desirable as they offer i) model definition on the basis of simple 1D material response models and structure geometry, ii) the potential for accurate simulation of system response (for flexure-controlled systems), and iii) more moderate computational demands than continuum elements. The primary focus of the first part of this study was to evaluate the accuracy with which this conventional modeling approach simulates the response of flexural walls.

Formulations

The OpenSees platform (http://opensees.berkeley.edu) and the distributed-plasticity beam-column element formulations available in that platform were employed for the current study. Both the displacement- and force-based element formulations were studied. Figure 4 shows schematics of a model of a cantilever wall, one employing force-based elements and one employing displacement-based elements. For both element formulations, a fiber-type section model and 1D concrete and steel constitutive models were used to simulate nonlinear flexural response; for both element formulations a linear shear response model was incorporated into the model. A mesh refinement study by Pugh (2012) indicated that a section model employing 32 concrete fibers within the boundary element and similarly sized fibers within the web of the wall was required to produce a converged solution for the section. Results are presented for different levels of mesh refinement at the element level (i.e. number of elements and number of fiber sections per element).

For the fiber sections, nonlinear material response was defined using typical 1D concrete and steel response models (Figure 5). Concrete response was defined using the Yassin model (1994) which is implemented in OpenSees as *Concrete02*. Using this model, pre-peak response in compression is defined by the Hognestad model (), post-peak response in compression is linear to a residual compressive strength, tensile response is bilinear to a residual tensile strength of zero, the unloading path from the compression envelope is bi-linear and from the tension envelope is linear, reloading paths are linear, and reloading in tension and compression occurs immediately upon unloading to a state of zero stress. To define parameters in Figure 5 for a specific test specimen, i) the reported concrete compressive strength (fc) was used, ii) concrete strain at peak strength (e0) was defined such that the concrete modulus at zero strain (Ec) was equal to that defined by ACI 318 (2011), iii) for confined concrete parameters K and e_{20} in Figure 5 were determined using the recommendations of Saatcioglu and Razi (1992), iv) for unconfined concrete e_{20} = 0.008, concrete tensile strength as defined equal to $0.33\sqrt{f_c'}$ MPa $\left(4\sqrt{f_c'}\ \text{psi}\right)$ per Wong and Vecchio, and v) concrete post-peak stiffness in tension was defined equal to Ec/20 per Yassin (1994).

The OpenSees *Steel02* material model was used to simulate the cyclic response of reinforcing steel (Fillipou et al. 1983). This model employs a bilinear envelope with unload-reload paths defined using Mengetto-Pinto curves. Figure 5 shows a cyclic strain history. Parameters defined in Figure 5 were taken directly from the reported materials properties for each specimen in the database. The OpenSees *MinMax* material model was used with the *Steel02* model to simulate loss of tensile strength when steel tensile strain exceeded the measured rupture strain and to simulate loss of compressive strength when steel compressive strain exceeded that resulting in 80% strength loss for surrounding concrete (e_{20} in Figure 5a).

Because the fiber-type section model does not simulate deformation due to shear, a shear response model was incorporated into the force- and displacement-based element models. The shear response is incorporated using two different approaches, depending on the type of element formulation. The displacement-based beam-column element formulation assumes Bernoulli-Euler beam theory, and a shear spring was introduced in series with the beam-column elements at each story (Figure 4). For the force-based beam-column element, a shear-response model was incorporated at the section level. The shear response of the wall was assumed to be linear elastic, with $V = \gamma G_{eff} k_s A_{cv}$ where V is the shear force on the section, γ is the shear strain on the section, G_{eff} is the effective shear modulus of the section, k_s the shear form factor taken as 5/6 for rectangular walls, and A_{cv} is the shear area of the section. For the current study, $G_{eff} = 0.1G_c = 0.04E_c$, where E_c is the elastic modulus of concrete defined per ACI 318 (2011) (Lowes et al. 2009). For the force-based element, shear response at the section is defined by the V-γ relationship. For the displacement-based element, a shear load versus lateral displacement (V-Δ_v) relationship is required for the shear spring placed at each story; this was defined on the basis of $\Delta_v=\gamma H$ where H is the height of the specimen.

Evaluation

The response of the wall specimens in Table 1 was simulated using the basic model. Three levels of mesh refinement were employed each for models comprising displacement-based elements and force-based elements. Analysis results were evaluated on the basis of the accuracy which the following quantities were simulated: (1) secant stiffness to the theoretical yield force, (2) maximum base shear force, and (3) drift capacity, defined as the drift corresponding to loss of 80% of the lateral-load carrying capacity. Table 2 presents these data, with simulated results normalized by measured results, for all of the specimens in the database. Additionally, Figure 6 shows simulated and measured force versus drift response for the four selected specimens. In Figure 6, shear force is normalized by the ACI shear strength (V_n) (ACI 318 2011) and drift is defined as the lateral displacement at the top of the specimen normalized by the specimen height.

The mesh refinement study was conducted to evaluate the number of elements and integration points needed to provide a converged solution. To study the effects of mesh refinement on displacement-based element models, meshes of 4, 8 and 16 elements were used to model the full height of the specimen. Five (5) fiber sections (i.e., integration points) were used for each displacement-based element. For the force-based element, meshes comprising a single force-based element including 3, 5 and 9 fiber sections (i.e. integration points) were used to model the full height of the specimen.

Table 3 presents the results of the mesh refinement study for all of the wall specimens; specimen data are organized on the basis of failure mode, which include compression failure (CB), bar rupture following buckling (BR), and bar rupture. The results differ depending on the mesh refinement and the element formulation. The tables show the predicted values for the displacement-based formulation element model in the leftmost columns and the force-based formulation model in the rightmost columns. Both are evaluated below.

The results indicate that accurate simulation of the yield stiffness and strength was achieved regardless of the mesh size. For the different element formulations and levels of mesh refinement, the mean ratio of simulated to measured yield stiffness ranged from 0.98 to 1.03 and the mean ratio of simulated to measured strength ranged from 0.97 to 1.06; coefficients of variation did not exceed 0.11. For the displacement-based element model, increased mesh refinement did improve the accuracy of simulated response. For the force-based element, improvement in accuracy was observed as the number of

elements increased from three (3) to five (5), but meshes employing five (5) and seven (7) elements generated essentially the same results.

The data in Table 3 and the response histories for the selected specimens shown in Figure 6 show also that both element formulations exhibit significant mesh sensitivity in prediction of drift capacity. These data show that more highly refined meshes, with more integration points (i.e. fiber sections) or more elements, predicted reduced drift capacity and more rapid strength loss.

To investigate the observed mesh sensitivity, section behavior was considered for the force-based element (Figure 7). Figure 7a and b show, for the force-based element, the simulated curvature profiles up the height of the wall for three levels of mesh refinement at two drift demand levels: just beyond the yield of the longitudinal reinforcement (Figure 7a) and just following the onset of strength loss (Figure 7b). Figure 7c and d show the simulated force versus drift history up to the point at which the curvature profiles are simulated.

The data in Figure 7b show that mesh sensitivity in simulated drift capacity results from localization of deformations at a single critical section. Comparing Figure 7a and b shows that this localization is unique to the softening regime. For the hardening portion of the curve (Figure 7a and c), mesh refinement simple results in a more accurate representation of the curvature profile up the height of the wall. However, for the softening portion of the curve (Figure 7b and d), mesh refinement results in larger curvature demands occurring over a shorter height of the column. Strength loss at a single critical section results in increased deformation at that softening section and elastic unloading, and thus reduced deformation, at the other sections. For a hardening system, increased deformation at the critical section is accompanied by increased strength, which results in the spread of yielding and increased load and deformation at other sections.

Reinforced concrete walls typically exhibit a softening-type response at larger drift demands because response is determined by concrete crushing and/or buckling of longitudinal reinforcement (Figure 1a). The data in Figure 2 show that almost 60% of the wall test specimens surveyed by Birely (2012) exhibited compression damage modes. In the database assembled for this study (Table 1), 19 of the 21 specimens are impacted by compressive response of concrete and steel and 12 specimens exhibit compression-controlled failure. Thus, structural reinforced concrete walls that are part of the lateral load resisting system may be expected to exhibit a softening-type response. Further, it should be expected that traditional analysis methods will result in simulation of wall response that is mesh-sensitive, with drift capacity and the rate of strength loss determined entirely by the level of mesh refinement employed in the model.

In addition to demonstrating mesh-sensitive drift capacity results, the data in Table 3also show that maximum strength as predicted using the displacement-based element formulation converges relatively slowly with increasing number of elements and that a relatively large number of elements are required to accurately simulate laboratory results. This is unexpected given that model strength is defined by the fiber-section flexural response, which is identical for all models and meshes considered. A closer look at the results reveals the extreme variability in the axial load distribution within the displacement-based element model (Figure 8). These data show that at a low level of mesh refinement (4 elements) simulated axial load at a section that varies between 40% and 160% of the applied constant axial load and that even for a highly refined mesh (32 elements) simulated axial load at a section varies between 75% and 110% of the applied constant axial load. For the displacement-based element formulation, this variation in axial load at the section occurs despite the fact that the resultant axial load for the element

is equal (within the solution tolerance) to the globally applied axial load. This is due to the fact the displacement-based element formulation assumes a constant axial strain at each section along the length of the element and that equilibrium is satisfied on average within the element. Since axial load at the section level affects the flexural strength of the section, the variation in axial load along the length of the element results in variation in element flexural strength. While increasing the number of elements reduces the section-level variation in axial load, axial load variation for practical levels of mesh refinement (i.e. 12 to 16 elements) was found to be sufficiently large that it affected modeling recommendations. For these reasons, the displacement-based element formulation was not used in the remainder of the evaluations or model development study.

The potential for distributed plasticity beam-column elements to exhibit mesh-sensitivity due to localization of deformation at a single softening section has been identified previously (Coleman and Spacone 2001). However, to date, distributed plasticity elements have been used primarily to simulate the response of concrete and steel beams and columns that exhibit a hardening-type response out to large drift demands. Typically, failure of these components is either not simulated, with system failure defined via post-processing of analysis results, or is simulated via steel fracture in tension, in which case the critical section exhibits catastrophic strength loss. However, this approach is not acceptable for full building or collapse analyses. Therefore an explicit method to evaluate the drift capacity of these important components is required.

MATERIAL MODEL REGULARIZATION TO LIMIT MESH SENSITIVITY

Prior research has identified the potential for mesh-sensitive simulation results such as those presented above (Coleman and Spacone 2001). However, it is not standard practice to regularize material response models in simulation of RC components using line-element type models. There are several reasons for this. The most important is the expectation that reinforced concrete components designed to meet current ACI Code requirements will exhibit a hardening-type response out to large drift demands at which point bar rupture results in catastrophic strength loss, thereby making material regularization unnecessary. However, experimental data () show that most RC walls do not exhibit a hardening-type response out to large drift but instead exhibit softening at moderate drifts.

To limit mesh sensitivity, it is common practice in continuum analysis of plain and reinforced concrete components to regularize the concrete post-peak tensile stress-strain response model using the concrete fracture energy, G_f, (cite FIB and another method for experimental determination of G_f) in combination with a mesh-dependent characteristic length. Regularization of concrete compressive response is also common in continuum analysis, though methods and energy values used in the process vary (). Coleman and Spacone (2001) extended the regularization approach used for continuum analysis to line-element analysis, recommending regularization of the 1D constitutive model used to simulate concrete compressive response in the fiber-section model for components that exhibit a softening moment-curvature response at the section level. Coleman and Spacone (2001) applied the proposed regularization approach to model the response of a cantilever column subjected to lateral and axial loading by Tanaka (1990) as reported by Taylor et al. (1997). The column was modeled using a single FBBC element and meshes with 4, 5 and 6 fiber sections. Bilinear steel response with 1% hardening was used for the reinforcement and the concrete material response was modeled using a Park-Kent model with material regularization. Unconfined confined concrete fibers were assigned a crushing energy of 25 N/mm based on recommendations by Jansen and Shah (1997) and the confined core concrete was assigned a value six times larger than this (150 N/mm) to account for the enhanced response provided by the transverse reinforcement. Results presented by Spacone and Coleman (Figure 9) show the

proposed material regularization procedure significantly reduced the mesh dependent softening response and enabled objective numerical simulation of the post-peak response.

For simulation of structural walls, there are four material response modes that must be considered: concrete subjected to tension, plain concrete subjected to compression, confined concrete subjected to compression, and reinforcing steel subjected to compression or tension. Figure 10 shows the approach adopted in this study for regularizing each of these as well as the definitions of the concrete fracture energy (G_f) unconfined concrete crushing energy (G_{fc}) confined concrete crushing energy (G_{fcc}) and steel hardening energy (Gs) used in the regularization process. In Figure 10, L_{IP} is the length associated with the fiber section (i.e. integration point) for which the material model is used. Given energy values G_f, G_{fc}, G_{fcc} and G_s as well as L_{IP}, the concrete and steel stress-strain response envelopes can be regularized.

For concrete tensile response, any of several experimental procedures and empirical models may be used to determine concrete fracture energy, G_f (CEB-FIP, 1990). For concrete response in compression, there are no current standard practices for experimental testing to determine G_{fc} or G_{fcc} and few empirical models are found in the literature. Two studies addressing crushing energy are: Jansen and Shah (1997) who recommend a value of 25 N/mm for normal-weight concrete, and Nakamura and Higai (1999) who define crushing energy for unconfined concrete to be a function of compressive strength such that normal-weight concrete has G_{fc} = 80 N/mm. Coleman and Spacone (2001) employed the G_{fc} value recommended by Jansen and Shah for unconfined concrete and recommend a value of $G_{fcc} = 6Gf_c$ for confined concrete; however, these values are not verified through comparison of simulated and measured response for typical reinforced concrete components.

Steel exhibits a hardening-type response. Thus, localization of deformation would be not expected in a fiber-type beam-column element model of a steel beam or column; instead material hardening would ensure distributed yielding along the length of the beam-column element. However, for a reinforced concrete section in which concrete crushing results in softening of the critical section, concrete and *reinforcing steel* deformations do localize. Thus, steel strain demands at the critical section are affected by mesh refinement and regularization of the steel material response is required to achieve mesh objective results. Given the hardening energy (G_s) and basic material response parameters as well as L_{IP}, a post-yield hardening modulus can be defined for reinforcing steel. Only one study addressing regularization of steel response for analysis using distributed plasticity elements was found in the literature (Chiaramonte 2011); Coleman and Spacone (2001) do not address regularization of steel response.

The following sections summarize the energy values and the methods used in this study to determine these values as well as compare results generated using the basic model with those generated using regularized material models.

Determination of Steel Post-Yield Energy

For RC components that exhibit softening at the section level, regularization of the steel as well as concrete material response is required. This is because section softening results in localization of inelastic deformation at a single critical section, and strain demands for both steel and concrete fibers are affected by this localization of deformation demands.

To determine a post-yield energy for use in regularizing reinforcing steel response, an approach often employed for continuum analysis of unconfined concrete responding in compression was adopted. For the reinforcing steel, the post-yield energy, G_s, was defined to be equal to the area under the

experimentally determined post-yield stress-strain history multiplied by the length over which inelastic deformation localizes, which was assumed equal to the gage length, L_{gage}, used in the laboratory. This is illustrated in Figure 10d. Thus,

$$G_s = \frac{1}{2}\left(\varepsilon_{u\_exp} - \varepsilon_y\right)\left(f_u + f_y\right)L_{gage} \quad \text{(Eq. 1)}$$

where ε_{u_exp} is the strain at ultimate strength, f_u, as determined from laboratory testing and all other parameters are as previously defined. To determine the strain at ultimate strength, ε_u, used in defining the regularized model, post-yield energy is assumed to be dissipated over the integration length used in the model (Figure 10d):

$$\varepsilon_u = \varepsilon_y + \frac{2}{(f_u + f_y)}\frac{G_s}{L_{IP}} = \varepsilon_y + \left(\frac{L_{gage}}{L_{IP}}\right)\left(\varepsilon_{u\_exp} - \varepsilon_y\right) \quad \text{(Eq. 2)}$$

where all variables are as defined previously. Thus, as the mesh becomes more highly refined and L_{IP} is reduced, the hardening modulus for the reinforcing steel is also reduced and larger strains are required to achieve a post-yield stress level.

It should be noted that the gage length used in steel material testing was not available for all of the test specimens in the data set. However, sensitivity studies performed on specimens experiencing crushing failures suggest results are not particularly sensitive to reasonable variations in the gage length used to regularize steel response. Analyses of crushing specimens were performed considering gage lengths between 100 and 760 mm. Over this range of gage lengths, simulated system response quantities (stiffness, peak strength, drift capacity) varied by less than 5**%** (Pugh 2012). For the analyses in which a gage length was not reported, a length of 200 mm (8 in.) was used for numerical modeling of wall specimens. This length is the gage length required per ASTM A370 (Methods for Testing Steel Reinforcing Bars).

For the regularized steel material model, the OpenSees *MinMax* material was used to simulate strength loss due to fracture under tensile loading and buckling under compressive loading. The regularized steel tensile strain at onset of strength loss was computed using an approach identical to that presented in Eq. 2. The regularized steel compressive strain at onset of strength loss was determined by the regularized concrete strain at 80% strength loss.

Determination of Unconfined and Confined Concrete Crushing Energy

The response of a wall with poorly confined concrete will be determined by the compressive response of the unconfined concrete. Since standardize tests do not exist for determining the crushing energy, Gfc, required to regularize the concrete constitutive model and define unconfined concrete compressive response, G_{fc} was determined using laboratory data from tests of walls with poorly confined concrete exhibiting compression-controlled failure. Specifically, load-displacement data for Specimen WSH4 and Specimen WR0 were used to determine the crushing energy for unconfined concrete. These were the only wall test specimens constructed entirely of unconfined concrete and exhibiting a compression-controlled failure.

To determine G_{fc}, a series of analyses were run of the WSH4 and WRO specimens using the basic force-based element model described above with material regularization. In these analyses, the unconfined concrete crushing energy, G_{fc}, was varied with the result that the strain at onset of residual compressive strength, $\varepsilon_{20u,}$ varied:

$$\varepsilon_{20u} = \frac{G_{fc}}{0.6 f_p L_{IP}} - \frac{0.8 f_p}{E_0} \quad \text{(Eq. 3)}$$

Figure 11 shows a plot of simulated to observed drift capacity as a function of G_{fc}/f_c. On the basis of these data, the crushing energy recommended for use with the force-based element (FBE) was determined to be

$$G_{fc} = 2 f_c' \text{ N/mm} \quad \text{(Eq. 4)}$$

A similar approach was used to determine an appropriate confined concrete crushing energy, G_{fcc}. A series of analyses were done of the ten walls from the database with confined concrete that exhibited compression-controlled failure. The basic force-based element model with material regularization was used. Unconfined concrete material response was regularized using Eq. 4. for the analyses. A range of confined concrete crushing energies were used.

Figure 12 shows the results of these analyses, with the ratio of simulated to predicted drift capacity plotted versus $K_c = G_{fcc}/G_{fc}$ with data grouped by boundary element confinement configuration. The data in Figure 12 show that for all cases, except the PW4 specimen, an increase in confined concrete crushing energy relative to unconfined concrete crushing energy is required to accurately simulate drift capacity. The data in Figure 12**Figure 12** show also that, with the exception of PW4, $K_c = G_{fcc}/G_{fc}$ increases with increasing confinement. Walls with rectangular boundary elements and crossties restraining all longitudinal reinforcement have the largest K_c values (average $K_c = 2.30$) with confinement providing a significant enhancement of concrete post-peak strain capacity while a wall with a rectangular boundary element with no crossties has the smallest K_c value ($K_c = 1.15$) with confinement providing minimal enhancement of concrete post-peak strain capacity. Walls with square boundary elements fall in the middle of this range with an average K_c of 1.45. On the basis of the data presented in Figure 12, confined concrete crushing energy was defined as follows:

$$G_{fcc} = 1.70 G_{fc} \quad \text{(Eq. 5)}$$

While the data in Figure 12 suggest that G_{fcc} is a function of confinement configuration, the data in Figure 12 were deemed to be insufficient to develop a predictive model.

Comparison of the Basic and Regularized Models

Figure 13 shows measured and simulated results for two specimens that responded in a compression buckling (CB) mode, Specimens WSH4 and OhWR0. The response of each specimen was simulated using a single force-based element with 5, 7 and 9 fiber sections; for each level of mesh refinement, four different sets of constitutive models were employed. Figure 13a and b show simulated results with no material regularization. Figure 13c and d show results for concrete material regularization in tension and compression and with no regularization of reinforcing steel response. Figure 13e and f show results with concrete and steel material regularization. On the basis of these results, the following conclusions and recommendations are made:

1. For a component that exhibits softening response, refining the mesh without material regularization results in more rapid degradation of the post-peak response.

2. Regularization of the concrete response in tension is not required for reinforced component with a flexural strength that exceeds the cracking strength (i.e., components for which the tensile response of the concrete does not control the post-peak behavior).

3. Regularization of the steel and concrete compression models (confined and unconfined) is required to achieve objective response prediction of softening specimens.

EVALUATION OF THE MODEL USING PROPOSED REGULARIZED CONSTITUTIVE MODELS AND PLANAR WALL DATA

To evaluate the modeling approach described above, simulated and measured base shear versus drift histories were compared for all of the walls listed in Table 1. Note specimens exhibiting CB failure modes (12 of 21 specimens) were used to calibrate the model. Simulations were conducted using the OpenSees platform. Although in the full study, two models were used to simulate each of the cantilever wall specimens, one comprising displacement-based elements and one comprising a single force-based element, only the force-based elements are presented here because of the issues noted with the axial load variation. Pugh (2012) presents results for the DBE models.

For the force-based elements, a three-element mesh was used with intra-element mesh discretization levels of 3, 5 and 7 fiber sections along each element. Each fiber-type sections employed 32 fibers within the confined boundary elements and fibers of similar thickness within the web of the walls. Unconfined and confined concrete material response was regularized using the recommended regularization values provided in Table 4. Analyses were conducted under displacement control using the displacement history imposed the laboratory. The boundary conditions and load patterns applied in the laboratory were represented in the simulations, with one exception. Walls that were subjected to a distributed lateral loading in the laboratory were subjected to a single lateral load at the top of the wall in the analysis. Results of a preliminary study comparing models in which the distributed load was simulated exactly and was approximated using a single point load at the top of the wall and indicated that this aspect of the model had essentially no impact on critical response quantities (Pugh 2012).

The results of the study are presented in tabular form in Table 5. Figure 14 presents the simulated and measured results of the validation study for the four selected specimens, which vary in damage mode and shear demand-capacity ratio. Using the data in Table 5, the following summarizes the regularized modeling approach:

1. Peak base shear strength of all walls was accurately simulated by all force-based element meshes considered. The mean simulated to observed peak strength ratio was 0.94 with a coefficient of variation of 0.04 for compression controlled wall specimens and 0.99 with a coefficient of variation of 0.06 for tension controlled specimens.

2. Secant stiffness values to yield for walls failing due to flexural compression (CB) and flexural tension (BR) were accurately simulated by all force-based element meshes considered. The mean simulated to observed yield stiffness ratio was 1.02 with a coefficient of variation of 0.10 for compression controlled wall specimens and 1.02 with a coefficient of variation of 0.09 for tension-controlled specimens.

3. Drift capacity data for walls failing due to flexural compression (CB) show some dependency on the number of integration points (Table 3). The ratio of simulated to observed drift capacity for models using three (3) fiber sections was 0.99 with a coefficient of variation of 0.17. The mean simulated to observed drift capacity ratio for models using seven (7) fiber sections was 1.06 with a coefficient of variation of 0.23. However, as indicated in Figure 15 and comparing the data presented in Tables 2 and 4, this is a vast improvement over the basic model.

4. For the two (2) specimens failing due to tension rupture prior to significant buckling (R), simulated-to-observed drift capacity ratios were slightly overestimated, with a mean simulated to observed drift capacity ratio of 1.11 for the five (5) fiber-section model. Drift capacity data for these specimens also show some mesh dependency; however, the mesh dependency is substantially less than that observed for the basic model.

5. For five (5) specimens failing due to tension rupture after significant buckling (BR), simulated to observed drift capacity ratios were slightly overestimated (ratios ranged from 1.06 to 1.11 for models with three, five and seven sections), the coefficient of variation for these ratios was relatively high (ratios ranged from 0.29 to 0.22), and some mesh dependency was observed. These results are likely due to the simplicity with which strength deterioration due to buckling of reinforcing steel was simulated.

Use of Simulated Response Quantities to Assess Performance

Regularization of material response provides a means of limiting mesh sensitivity and enabling accurate simulation of drift capacity for walls, and other reinforced concrete components, for which material softening produces section softening and, ultimately, component strength loss. However, material regularization does limit the manner in which simulated material response data can be used to assess component performance. Specifically, simulated concrete and steel strain data cannot be directly compared with material test data; a maximum simulated unconfined concrete compressive strain of 0.003 mm/mm or a maximum reinforcing steel tensile strain of 0.2 mm/mm is not relevant and must be reassessed.

However, simulated concrete and steel stress-strain data can be evaluated in relative terms to assess performance. For example, a concrete strain resulting in a specified percentage loss in compressive strength could be used to define a performance state characterized by concrete crushing and a maximum steel tensile strain equal to 100 times the yield strain could be used to define a performance state characterized by steel fracture. In this study, the regularized concrete strain resulting in an 80% loss in compressive strength at the critical fiber section was used to define concrete crushing and a maximum steel tensile strain equal to 100% of the regularized rupture strain was used to define a strain limit characterizing steel rupture.

For each specimen model, the extreme fiber concrete compressive strain (negative value) and the maximum extreme fiber steel strains strain were determined at the load step for which the simulated drift capacity was reached. The peak strain values were then compared to the strain limit values. The computed strain was normalized to the limiting strain values. If the compressive strain ratio exceeded 1.0, a crushing failure mode was identified. Table 5 presents the identified failure modes. The results are as follows. For the specimens that exhibited a crushing following bar buckling (CB) failure in the laboratory, the predicted failure mode was also identified as crushing. For the remaining specimens, the modeling predicted the observed damage mode correctly for the majority of the specimens (4 of 5 for the BR failure mode and 1 of 2 for the R failure mode).

EVALUATION OF THE MODEL USING PROPOSED REGULARIZED CONSTITUTIVE MODELS AND NON-PLANAR WALL DATA

To further evaluate the modeling approach described above, simulated and measured base shear versus drift histories were compared for selected non-planar walls listed in Table 2. Simulations were conducted using the same modeling approach as used for the planar wall evaluation study described

above; however, analyses were done using only the OpenSees force-based element with 7 fiber sections. Ratios of simulated to measured secant stiffness to yield, maximum strength and drift capacity are presented in tabular form in Table 5; note that for each specimen the largest or smallest ratio for all loading directions, with represents the largest simulation error, is listed. Figure 16 presents the simulated and measured results of the validation study for the two selected c-shaped wall specimens; Figure 17 presents the simulated and measured results of the validation study for the two selected t-shaped wall specimens. The data in Table 5 and Figures 16 and 17 support the following observations:

1. For c-shaped wall specimens, the regularized modeling approach provides accurate simulation of secant stiffness to yield, maximum strength and drift capacity. For these response quantities, the average ratio of simulated to measured response ranged from 0.96 to 1.00 and coefficients of variation range from 8% to 20%. However, for specimens W2 and W3, the ratio of simulated to measured drift capacity was 0.77 and 0.70, respectively. Thus, there is the potential for the model to provide inaccurate prediction of drift capacity.

2. For t-shaped wall specimens, the regularized modeling approach does not provide accurate simulation of response. On average, strength is accurately predicted; however, for one of four specimens, the ratio of simulated to measured strength is 1.25. This is a significant error. Secant stiffness to yield and drift capacity are poorly predicted, average ratios of simulated to measure response range from 0.64 to 1.55 and ratios for individual specimens range from 0.42 to 2.40.

3. Qualitative evaluation of the load versus drift histories presented in Figures 16 and 17 suggests that the regularized model provides acceptably accurate simulation of cyclic response quantities such as unloading stiffness, reloading stiffness and energy dissipation.

4. Results do not suggest that inaccuracy in response simulation is associated with bidirectional loading.

Thus, the data in Table 5 and Figures 16 and 17 suggest that the model is appropriate for use in simulating the response of c- but not t-shaped walls. The data suggest also that further evaluation, using an expanded data set, is required to fully validate the model for simulation of c-shaped walls and improve understanding of application of the model for simulation of t-shaped walls. Finally, the data suggest that further evaluation of the model using an expanded data set that includes also other non-planar wall configurations (e.g. L- and H-shaped walls) is warranted.

Simulation error for non-planar walls is attributed to the assumptions employed in the fiber-type beam-column element formulation. Specifically, the element formulation employs the assumptions of a linear axial strain gradient, and thus a constant shear strain, on the member cross section and decoupling of flexure and shear response at the material level. These assumptions could be expected to result in inaccurate simulation of response for walls for which shear response, manifested as large nonlinear shear deformations and/or material damage due to combined shear and flexural demands, is significant. For both c- and t-shaped walls, experimental data (Lowes et al. 2013, Thomsen and Wallace 2004) show that there is a nonlinear axial strain gradient on the member cross section due to shear. For the c-shaped walls considered here, nonlinearity in the strain gradient is not sufficient to impact global load-deformation response. For the t-shaped walls considered here, it is.

SUMMARY AND CONCLUSIONS

Reinforced concrete walls are one of the most common lateral load resisting systems used regions of high seismicity. However, prior test results and post-earthquake reconnaissance efforts indicate that even walls that meet the ductile detailing and tension-controlled response requirements according to ACI 318-11 (ACI 2011) can exhibit a softening response mode and compression-controlled failure. Therefore, performance evaluation of buildings that include these components requires computationally efficient nonlinear models that accurately capture this softening behavior.

The research presented here considered standard modeling techniques, evaluating and ultimately improving the accuracy with which these models simulate the response of slender RC walls. The models were evaluated using a dataset of 21 slender planar walls tested in the laboratory by 7 research groups; wall specimens exhibited a range of failure modes. Two nonlinear beam-column element formulations were evaluated, a displacement-based formulation and a force-based formulation; both element formulations employed fiber-type sections models with standard 1D constitutive models for concrete and steel. Both element formulations were found to provide accurate and precise simulation of stiffness and strength for the planar wall specimens. However, both formulations were also found to exhibit mesh-sensitivity in simulating drift capacity, with increasing mesh refinement resulting in reduced drift capacity and increasingly rapid strength loss. Additionally, the displacement-based formulation was found to produce significant errors in the axial load distribution along the length of the element and, thus, was regarded as inherently inaccurate.

To minimize mesh-sensitivity and provide accurate simulation of drift-capacity, the 1D concrete and steel constitutive models were regularized. Energy values used for regularization of unconfined and confined concrete compression response were developed using data from a limited set of prior planar wall tests. Energy values used for regularization of reinforcing steel response were developed from material test data. Results show that the forced-based beam-column element, with the regularized material models, provides accurate simulation of stiffness, strength and drift capacity with minimal mesh-sensitivity for planar walls.

The regularized model was evaluated using a dataset of 10 slender c-shaped and t-shaped RC walls. Results suggest that the model provides accurate simulation of stiffness, strength and drift capacity for c-shaped walls but does not provide accurate simulation of response for t-shaped walls. Inaccurate simulation of response is attributed to the simplifying assumptions inherent to the beam-column element formulation. Further evaluation of the model using experimental data for non-planar walls with a range of configurations and subjected to bidirectional is recommended.

ACKNOWLEDGEMENTS

The research presented herein was funded by the Charles Pankow Foundation and the National Science Foundation through the Network for Earthquake Engineering Simulation Research Program, Grant CMS-042157, Joy Pauschke, program manager. Any opinions, findings, and conclusions or recommendations expressed in this material are those of the authors and do not necessarily reflect the views of the Charles Pankow Foundation or the National Science Foundation.

REFERENCES

1. Bentz, E.C. (2000). "Sectional Analysis of Reinforced Concrete Members," *PhD Thesis*. Department of Civil Engineering, University of Toronto. 310 pp.

2. Beyer, K., Dazio, A. and Priestley, M. (2011). “Quasi-static cyclic tests of two U-shaped reinforced concrete walls,” *Journal of Earthquake Engineering*, 12: 1023–1053.

3. Boivin, Y. and Paultre, P. (2012). “Seismic force demand on ductile reinforced concrete shear walls subjected to western North American ground motions: Part 1 — parametric study” *Canadian Journal of Civil Engineering* (39): 723-737.

4. Brueggen, B.L. (2009). “Performance of T-shaped Reinforced Concrete Structural Walls under Multi-Directional Loading,” *Ph.D. Dissertation*, University of Minnesota.

5. Calugaru, V. and Panagiotou, M. (2012). “Response of tall cantilever wall buildings to strong pulse type seismic excitation,” *Earthquake Engineering and Structural Dynamics* (41): 1301–1318.

6. Commissariat a L’Energie Atomique (CEA) (2002). *IAEA CRP-NFE CAMUS Benchmark: Experimental results and specifications to the participants, Report CEA/SEMT/EMSI/RT/02-047/A and CD*. Commissariat a L’Energie Atomique (CEA), Direction De L’Energie nucleaire. 67 p.

7. Elwood, K.J., Matamoros, A. Wallace, J.W. Lehman, D.E. Heintz, J. Mitchell, A., Moore, M. Valley, M. Lowes, L.N., Comartin, C. and J.P. Moehle. “Update to ASCE/SEI 41 Concrete Provisions.” *Earthquake Spectra.* 23(3) (2007): 493-523.

8. Galal, K. (2008). “Modeling of Lightly Reinforced Concrete Walls Subjected to Near-Fault and Far-Field Earthquake Ground Motions,” *The Structural Design of Tall and Special Buildings* (17): 295–312.

9. Ghobarah, A., Galal, G., and Elgohary, M. (2004). “Dynamic Resposne of Lightly Reinforced Concrete Walls,” *Proceedings of the 13th World Conference on Earthquake Engineering, Vancouver B.C., Canada, August 1-6, 2004.* Paper No. 1090.

10. Giberson, M.F. (1969), “Two Nonlinear Beams with Definition of Ductility,” *Journal of the Structural Division, ASCE* 95(2): 137-157.

11. Ile, N. and Reynouard, J. (2005), Behaviour of U-shaped walls subjected to uniaxial and biaxial cyclic lateral loading, *Journal of Earthquake Engineering*, 9(1), 67-94.

12. Lowes et al. (2012). “Behavior, Analysis and Design of Complex Wall Systems,” http://nees.org/warehouse/project/104.

13. Massone (2006). “RC Wall Shear – Flexure Interaction: Analytical and Experimental Response,” *Ph.D. Disseration*, University of California, Los Angeles.

14. Palermo, D., Vecchio, F. J. (2002). “Behavior of three-dimensional reinforced concrete shear walls” *ACI Structural Journal* 99(1): 81-89.

15. Palermo, D., Vecchio, F. (2007). “Simulation of cyclically loaded concrete structures based on the finite-element method,” *Journal of Structural Engineering*, *ASCE* 133(5): 728–738.

16. Orakcal, K., Wallace, J.W., Conte, J.P. (2004). “Flexural modeling of reinforced concrete walls – model attributes” *ACI Structural Journal* 101(5): 688-698.

17. Rejec, K., Isakovic, T., Fischinger, M. (2012). “Seismic shear force magnification in RC cantilever structural walls, designed according to Eurocode 8,” *Bulletin of Earthquake Engineering* (10): 567-586.

18. Scott, M., Fenves, G.L. (2006). “Plastic hinge integration methods for force-based beam-column elements,” *Journal of Structural Engineering, ASCE* 132(2): 244-252.

19. Spacone, E., Ciampi, V., Filippou, F.C. (1996). “Mixed Formulation of Nonlinear Beam Finite Element,” *Computers and Structures* 58(1): 71-83.

20. Thomsen IV, J.A. and Wallace, J. W. (2004). “Displacement-Based Design of Slender REinfroced Concrete Structural Walls – Experimental Verification” *Journal of Structural Engineering, ASCE* 130(4): 618-630.

21. Vulcano, A.; Bertero; V. V.; and Colotti, V. (1988). “Analytical Modeling of RC Structural Walls,” *Proceeding, 9th World Conference on Earthquake Engineering, V. 6, Tokyo-Kyoto, Japan, 1988.* pp. 41-46.

22. Yassin, M. (1994). “Nonlinear analysis of prestressed concrete structures under monotonic and cyclic loads,” Ph.D. Dissertation. University of California, Berkeley.

23. Zeris, C., Mahin, S.A. (1988), “Analysis of reinforced concrete beam columns under uniaxial excitation,” *Journal of Structural Engineering, ASCE* 114: 804-820.

Table 1: Planar Wall Experimental Data Set

Specimen ID	Author	Load Type	l_w/t	$M/(Vl_w)$	$P/(A_g f'_c)$	$V_{max}/(A_{cv}\sqrt{f'_c})$ (MPa)	$V_{max}/(A_{cv}\sqrt{f'_c})$ (psi)	V_{max}/Vn	Δ_y (%)	Δ_u (%)	Failure Mode
WSH1	Dazio, et al.	UC	13.3	2.28	0.06	0.17	2.0	0.44	0.24	1.04	R
WSH2	Dazio, et al.	UC	13.3	2.28	0.06	0.19	2.3	0.53	0.27	1.75	BR
WSH3	Dazio, et al.	UC	13.3	2.28	0.06	0.24	2.9	0.67	0.32	2.07	BR
WSH4	Dazio, et al.	UC	13.3	2.28	0.06	0.23	2.8	0.62	0.29	1.60	CB
WSH5	Dazio, et al.	UC	13.3	2.28	0.14	0.23	2.8	0.59	0.20	1.52	BR
WSH6	Dazio, et al.	UC	13.3	2.26	0.11	0.30	3.6	0.83	0.31	2.04	CB
W1	Liu	UC	6.07	3.13	0.08	0.19	2.3	0.46	0.64	2.98	CB
W2	Liu	UC	6.07	3.13	0.04	0.14	1.7	0.37	0.55	2.91	BR
PW1	Lowes, et al.	UC	20.0	2.84	0.10	0.29	3.5	0.71	0.38	1.53	R
PW2	Lowes, et al.	UC	20.0	2.08	0.13	0.44	5.3	1.11	0.45	1.50	CB
PW3	Lowes, et al.	UC	20.0	2.00	0.10	0.37	4.4	0.88	0.24	1.22	CB
PW4	Lowes, et al.	UC	20.0	2.00	0.12	0.38	4.6	0.88	0.40	1.01	CB
RW1	Thomsen, et al.	UC	12.0	3.13	0.11	0.21	2.6	0.50	0.48	2.26	BR
RW2	Thomsen, et al.	UC	12.0	2.35	0.09	0.22	2.7	0.52	0.55	2.35	CB
R1	Oesterle, et al.	UC	18.8	2.35	0.00	0.09	1.1	0.23	0.15	2.30	BR
R2	Oesterle, et al.	UC	18.8	1.60	0.00	0.17	2.1	0.42	0.34	2.89	BR
S5	Vallenas, et al.	M	21.2	1.60	0.05	0.57	6.8	0.85	0.31	1.47	CB
S6	Vallenas, et al.	UC	21.2	2.00	0.05	0.53	6.4	0.80	0.32	1.65	CB
WR20	Oh, et al.	UC	7.50	2.00	0.10	0.25	3.0	0.76	0.35	2.82	CB
WR10	Oh, et al.	UC	7.50	2.00	0.10	0.24	2.9	0.65	0.47	2.82	CB
WR0	Oh, et al.	UC	7.50	2.00	0.11	0.25	3.0	0.74	0.52	2.14	CB

Table 2: Non-planar Wall Experimental Data Set

Specimen ID	Author	Shape	Load Dir.*	l_w/t	$M/(Vl_w)$	$P/(A_g f'_c)$	$V_{max}/(A_{cv}\sqrt{f'_c})$ (MPa)	$V_{max}/(A_{cv}\sqrt{f'_c})$ (psi)	V_{max}/V_n	Δ_y (%)	Δ_u (%)	Failure Mode
UW1	Lowes et al.	C	±X	20	2.84	0.05	0.33	4.0	0.51	0.34	1.86	CB
UW2	Lowes et al.	C	±X	20	2.84	0.05	0.36	4.3	0.41	0.35	1.50	BR
UW2			+Z		2.84	0.05	0.37	4.4	0.45	0.42		
UW2			−Z		2.84	0.05	0.22	2.6	0.27	0.63		
UW3	Lowes et al.	C	±X	20	2.84	0.05	0.33	4.0	0.41	0.35	1.80	BR
UW3			+Z			T	0.47	5.7	0.58	0.65		
UW3			−Z			C	0.68	8.2	0.84	0.65		
W1	Ile and Reynouard	C	±X	6	2.60	0.10	0.50	6.0	0.65	0.30	3.00	BR
W2	Ile and Reynouard	C	+Z	6	3.12	0.10	0.25	3.0	0.47	0.26	3.00	CB
W2			−Z		3.12	0.10	0.23	2.8	0.44	0.33	3.00	CB
W3	Ile and Reynouard	C	±X	6	2.60	0.10	0.50	6.0	0.61	0.43	2.00	BR
W3			+Z		3.12	0.10	0.19	2.3	0.39		2.00	BR
W3			−Z		3.12	0.10	0.23	2.8	0.47	0.34	2.00	BR
TUA	Beyer et al.	C	±X	8.7	2.58	0.02	0.27	3.2	0.79	0.40	3.50	BR
TUA			+Z		2.81	0.02	0.16	1.9	0.47	0.23	3.50	BR
TUA			−Z		2.81	0.02	0.14	1.7	0.41	0.35	3.50	BR
TUB	Beyer et al.	C	±X	13	2.58	0.04	0.47	5.7	0.99	0.36	3.00	CB
TUB			+Z		2.81	0.04	0.27	3.3	0.57	0.33	3.00	CB
TUB			−Z		2.81	0.04	0.23	2.8	0.49	0.35	3.00	CB
TW1	Thomsen and Wallace	T	+Z	12	3.0	0.09	0.40	4.9	1.05	0.5	1.24	CB
TW1			−Z	12	3.0	0.09	0.22	2.6	0.71	0.17	1.60	
TW2	Thomsen and Wallace	T	+Z	12	3.0	0.075	0.46	5.5	1.06	0.5	2.25	CB
TW2			−Z	12	3.0	0.075	0.24	2.9	0.55	0.15	2.43	
NTW1	Brueggen et al.	T	±X	12	4.3	0.03	0.27	3.3	0.37		3.3	CB
NTW1			+Z	15	3.5	0.03	0.50	6.0	0.68	0.34	1.8	
NTW1			−Z	15	3.5	0.03	0.26	3.2	0.36	0.28	1.1	
NTW2	Brueggen et al.	T	±X	12	4.3	0.03	0.25	3.0	0.33		3.1	CB
NTW2			+Z	15	3.5	0.03	0.55	6.6	0.73	0.25	2.1	
NTW2			−Z	15	3.5	0.03	0.30	3.6	0.40	0.19	1.4	

Note: 1. Loading direction: ±X indicates lateral loading parallel to the web of the c-shaped wall or the flange of t-shaped walls; response is nominally symmetric in the positive and negative loading directions; +Z / −Z indicates loading parallel to the flanges of the c-shaped walls or the web of the t-shaped wall; response is not symmetric, with +Z indicating loading putting the toes of the wall in compression and −Z indicating loading putting the toes of the wall in tension.

Table 3: Analysis Results for Planar Wall Specimens and Conventional Modeling Approaches

Specimen	Failure Mode	Displacement-Based									Force-Based								
		$k_{y,sim}/k_{y,obs}$			$V_{bm,sim}/V_{bm,obs}$			$\Delta_{u,sim}/\Delta_{u,obs}$			$k_{y,sim}/k_{y,obs}$			$V_{bm,sim}/V_{bm,obs}$			$\Delta_{u,sim}/\Delta_{u,obs}$		
		4 EL	8 EL	16 EL	4 EL	8 EL	16 EL	4 EL	8 EL	16 EL	3 IP	5 IP	7 IP	3 IP	5 IP	7 IP	3 IP	5 IP	7 IP
WSH4	CB	0.98	0.98	0.97	1.05	1.00	0.97	1.54	0.94	0.62	0.99	0.97	0.97	0.93	0.94	0.94	1.27	0.57	0.44
WSH6	CB	0.89	0.89	0.89	0.98	0.95	0.93	2.68	1.74	1.19	0.88	0.89	0.89	0.89	0.91	0.91	2.58	0.95	0.65
W1	CB	1.22	1.18	1.17	1.11	1.06	1.05	3.86	2.69	2.18	1.12	1.16	1.17	0.98	1.05	1.04	2.69	1.62	1.64
PW2	CB	1.01	1.00	1.00	1.04	1.01	0.99	3.00	1.89	1.38	0.99	1.00	1.00	0.96	0.98	0.98	2.33	1.13	1.00
PW3	CB	0.87	0.87	0.87	1.02	1.00	0.99	4.51	3.43	2.87	0.87	0.87	0.87	0.96	0.98	0.98	4.10	2.46	2.36
PW4	CB	1.05	1.05	1.05	1.28	1.24	1.23	4.93	3.77	3.24	1.04	1.04	1.04	1.20	1.20	1.21	3.48	2.88	2.81
RW2	CB	1.17	1.13	1.12	0.94	0.92	0.92	3.19	2.25	1.76	1.06	1.10	1.11	0.84	0.92	0.91	3.07	1.38	1.38
S5	CB	0.84	0.84	0.84	1.12	1.09	1.07	2.25	1.78	1.53	0.84	0.84	0.84	1.05	1.05	1.06	1.77	1.44	1.43
S6	CB	0.88	0.88	0.88	1.18	1.15	1.14	3.34	2.66	2.26	0.88	0.88	0.88	1.11	1.11	1.12	2.62	2.13	2.13
WR20	CB	1.05	1.01	1.01	0.97	0.93	0.92	1.37	0.80	0.52	1.01	1.00	1.01	0.89	0.90	0.90	1.25	0.47	0.31
WR10	CB	1.15	1.09	1.09	0.99	0.95	0.94	1.93	1.35	0.80	1.06	1.08	1.08	0.91	0.92	0.92	1.86	0.79	0.46
WR0	CB	1.18	1.16	1.12	0.99	0.96	0.94	0.92	0.56	0.39	1.09	1.11	1.10	0.91	0.92	0.92	0.76	0.34	0.27
Mean	CB	1.02	1.01	1.00	1.06	1.02	1.01	2.79	1.99	1.57	0.99	0.99	0.99	0.97	0.99	0.99	2.31	1.35	1.24
COV	CB	0.13	0.12	0.11	0.09	0.09	0.09	0.45	0.51	0.60	0.10	0.11	0.11	0.11	0.10	0.10	0.42	0.60	0.70
WSH2	BR	1.00	1.00	1.00	0.98	0.95	0.94	3.42	2.00	1.40	1.00	0.98	1.00	0.88	0.93	0.93	2.57	0.98	0.84
WSH3	BR	0.97	0.96	0.96	1.00	0.96	0.95	2.67	1.70	1.20	0.99	0.95	0.95	0.90	0.93	0.94	2.42	0.92	0.72
WSH5	BR	0.82	0.81	0.81	1.01	0.96	0.94	1.75	1.14	0.72	0.78	0.80	0.80	0.90	0.91	0.91	1.66	0.66	0.47
W2	BR	1.20	1.16	1.14	1.10	1.07	1.07	4.12	3.38	2.71	1.08	1.11	1.12	0.98	1.07	1.06	2.75	2.01	2.11
RW1	BR	1.12	1.11	1.10	1.02	0.99	0.99	2.85	1.98	1.48	1.06	1.08	1.09	0.91	0.98	0.97	2.76	1.11	1.10
R1	BR	0.96	0.97	0.96	1.13	1.10	1.09	3.48	3.48	3.22	0.88	1.00	0.94	1.04	1.05	1.05	3.47	2.93	2.82
R2	BR	1.17	1.14	1.13	1.17	1.14	1.14	2.77	2.77	2.77	1.09	1.11	1.12	1.10	1.11	1.11	2.77	2.71	2.68
Mean	BR	1.03	1.02	1.01	1.06	1.03	1.02	3.01	2.35	1.93	0.98	1.00	1.00	0.96	1.00	1.00	2.53	1.62	1.54
COV	BR	0.13	0.12	0.12	0.07	0.07	0.08	0.25	0.38	0.50	0.12	0.11	0.12	0.09	0.08	0.08	0.21	0.57	0.64
WSH1	R	1.00	1.00	1.00	1.05	1.01	1.00	3.36	1.95	1.39	0.98	0.99	1.00	0.94	0.97	0.97	2.56	1.08	0.79
PW1	R	0.99	0.99	0.99	1.06	1.04	1.03	2.88	1.95	1.53	0.98	0.99	0.99	1.00	1.01	1.01	2.22	1.31	1.20
Mean	R	0.99	1.00	0.99	1.06	1.02	1.01	3.12	1.95	1.46	0.98	0.99	0.99	0.97	0.99	0.99	2.39	1.20	1.00
Mean	ALL	1.02	1.01	1.00	1.06	1.02	1.01	2.90	2.11	1.67	0.98	1.00	1.00	0.97	0.99	0.99	2.43	1.42	1.31
COV	ALL	0.12	0.11	0.11	0.08	0.08	0.08	0.36	0.43	0.53	0.10	0.10	0.10	0.09	0.08	0.09	0.33	0.56	0.65

Table 4: Recommendations for Regularized Material Models for RC Wall Simulation

Material	Regularization Values
Longitudinal Reinforcing Steel	Equations 1 and 2
Concrete Subjected to Tension	Not required
Unconfined Concrete Subjected to Compression	$G_{fc}=2f'_c$ (N/mm)
Confined Concrete Subjected to Compression	$G_{fcc}=1.7G_{fc}$

Table 5: Comparison of Simulated and Observed Response Quantities for Planar Wall Specimens and Regularized Model

Specimen	Failure Mode	Force-Based											
		Stiffness Ratio			Strength Ratio			Drift Ratio			Failure Mode		
		3 IP	5 IP	7 IP	3 IP	5 IP	7 IP	3 IP	5 IP	7 IP	3 IP	5 IP	7 IP
WSH4	CB	0.96	0.96	0.96	0.95	0.95	0.95	1.05	1.05	1.13	C	C	C
WSH6	CB	0.95	0.95	0.95	0.91	0.92	0.92	0.80	0.70	0.70	C	C	C
W1	CB	1.16	1.17	1.18	1.02	1.01	1.02	1.00	1.00	1.00	C	C	C
PW2	CB	1.06	1.06	1.06	0.97	0.96	0.96	0.82	0.87	0.92	C	C	C
PW3	CB	0.95	0.95	0.95	0.93	0.93	0.93	0.95	1.00	1.08	C	C	C
PW4	CB	1.11	1.11	1.11	1.14	1.11	1.10	1.32	1.45	1.56	C	C	C
RW2	CB	1.14	1.15	1.15	0.90	0.88	0.87	1.13	1.21	1.32	C	C	C
S5	CB	0.87	0.87	0.87	0.98	0.97	0.97	0.70	0.86	1.05	C	C	C
S6	CB	0.91	0.91	0.91	1.03	1.00	0.99	1.16	1.23	1.30	C	C	C
WR20	CB	1.02	1.03	1.03	0.89	0.90	0.90	0.99	0.90	0.83	C	C	C
WR10	CB	1.05	1.08	1.07	0.92	0.93	0.93	1.01	0.99	0.96	C	C	C
WR0	CB	1.09	1.11	1.11	0.91	0.92	0.92	0.94	0.90	0.88	C	C	C
Mean	CB	1.02	1.03	1.03	0.96	0.96	0.96	0.99	1.01	1.06	-	-	-
COV	CB	0.09	0.10	0.10	0.07	0.06	0.06	0.17	0.20	0.23	-	-	-
WSH2	BR	1.02	1.02	1.01	0.93	0.92	0.91	0.93	1.15	1.27	R	R	R
WSH3	BR	0.98	0.98	0.98	0.93	0.93	0.93	0.89	1.00	1.00	C	C	C
WSH5	BR	0.84	0.84	0.84	0.92	0.93	0.93	0.83	0.72	0.72	C	C	C
W2	BR	1.08	1.11	1.10	1.05	1.03	1.02	1.58	1.37	1.37	C	C	C
RW1	BR	1.12	1.12	1.12	0.97	0.95	0.94	1.06	1.17	1.17	C	C	C
Mean	BR	1.01	1.01	1.01	0.96	0.95	0.95	1.06	1.08	1.11	-	-	-
COV	BR	0.11	0.11	0.11	0.06	0.05	0.05	0.29	0.22	0.23	-	-	-
WSH1	R	1.03	1.02	1.02	0.97	0.98	0.98	1.07	1.17	1.20	R	R	R
PW1	R	1.06	1.06	1.06	1.01	1.01	1.00	1.01	1.05	1.15	C	C	C
Mean	R	1.05	1.04	1.04	0.99	1.00	0.99	1.04	1.11	1.18	-	-	-
Mean	CB	1.02	1.03	1.03	0.96	0.96	0.96	1.01	1.04	1.08	-	-	-
COV	CB	0.09	0.09	0.09	0.07	0.06	0.06	0.20	0.19	0.21	-	-	-

Table 6: Comparison of Simulated and Observed Response Quantities for Selected Non-Planar Wall Specimens and Regularized Model

Specimen	Failure Mode	Shape	Load Dir.*	Stiffness Ratio	Strength Ratio	Drift Ratio
UW1	CB	C	±X	1.13	1.01	1.20
W1	BR	C	±X	0.85	0.90	1.00
W2	CB	C	+Z	0.87	0.94	0.77
W3	BR	C	±X	1.10	0.93	0.70
TUA	BR	C	±X	0.90	1.06	1.04
TUB	CB	C	±X	1.15	1.08	1.06
Mean				1.00	0.99	0.96
COV				0.14	0.08	0.20
TW1	CB	T	+Z	2.40	1.25	0.42
TW2	CB	T	+Z	1.60	1.00	0.45
NTW1	CB	T	±X	1.14	1.00	0.86
NTW2	CB	T	±X	1.05	0.95	0.82
Mean				1.55	1.05	0.64
COV				0.40	0.13	0.37

(a) Compressive Damage | (b) Tension Damage

Figure 1: Typical Damage Modes in Slender Walls

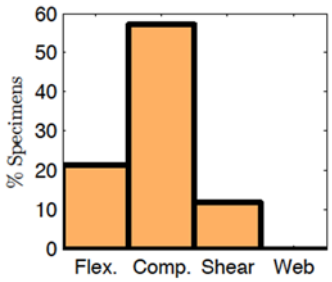

Figure 2: Percentage of Slender Rectangular Wall Specimens Exhibiting a Specific Damage Mode

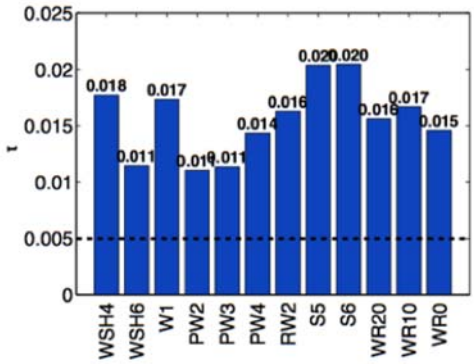

Figure 3: Tensile Strain at Nominal Strength

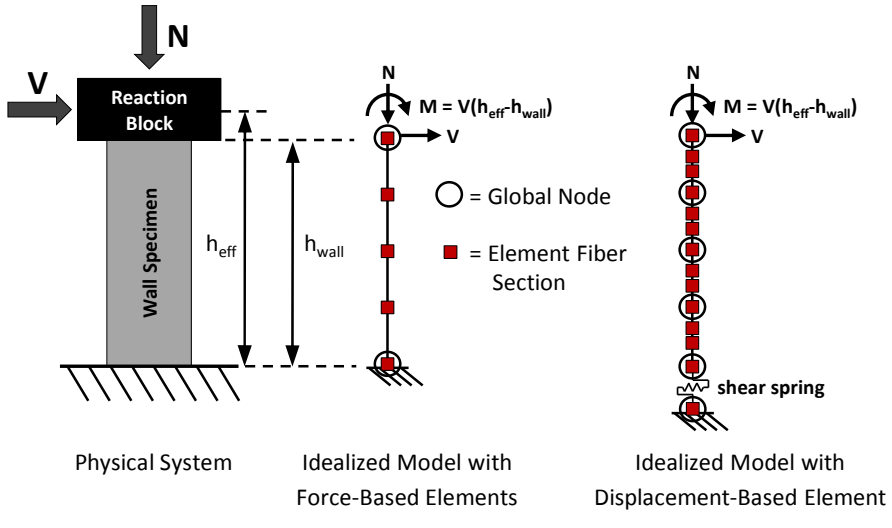

Figure 4: Typical Simulation Models for Test Wall

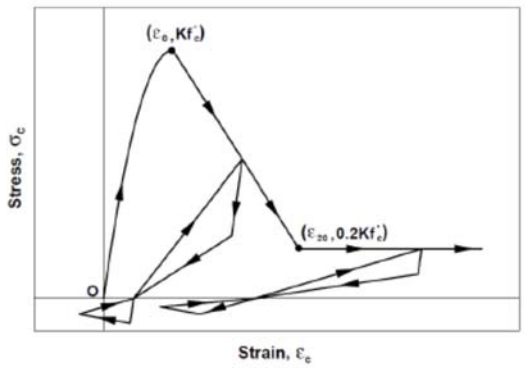

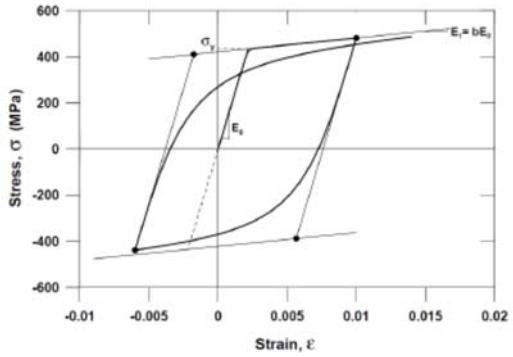

1D Concrete Model by Yassin (1994)	1D Steel Model by Fillipou et al. (1983)

Figure 5: Constitutive Models used for Basic Model

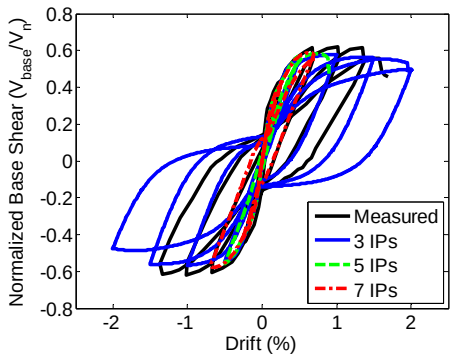

(a) WSH4, CB Failure, low shear stress demand

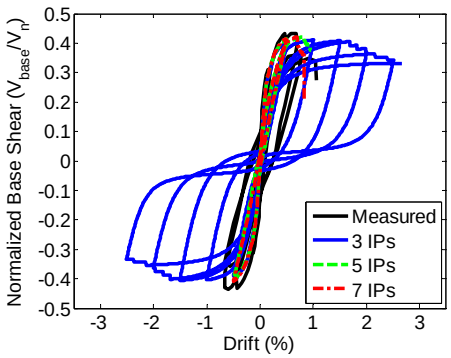

(b) WSH1, R Failure

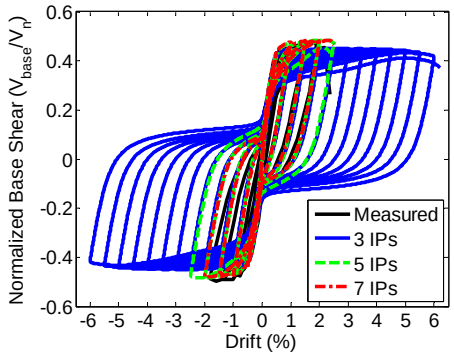

(c) RW1, BR Failure

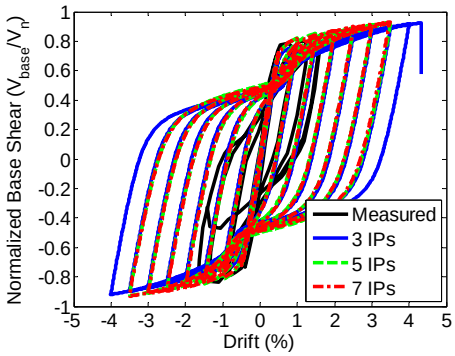

(d) S6, CB Failure, high shear stress demand

Figure 6: Predicted Responses of Highlighted Specimens with Basic Model.

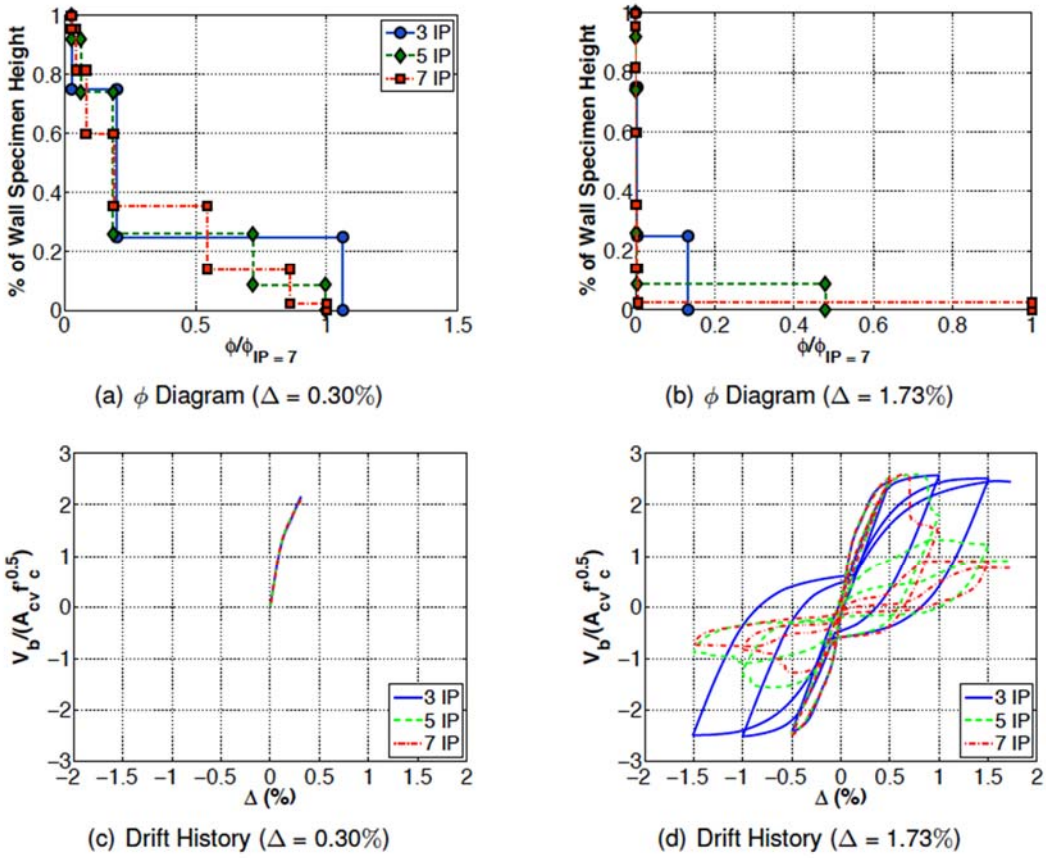

Figure 7: Local Deformation and Global Response of WSH4 Using Force-Based Formulation

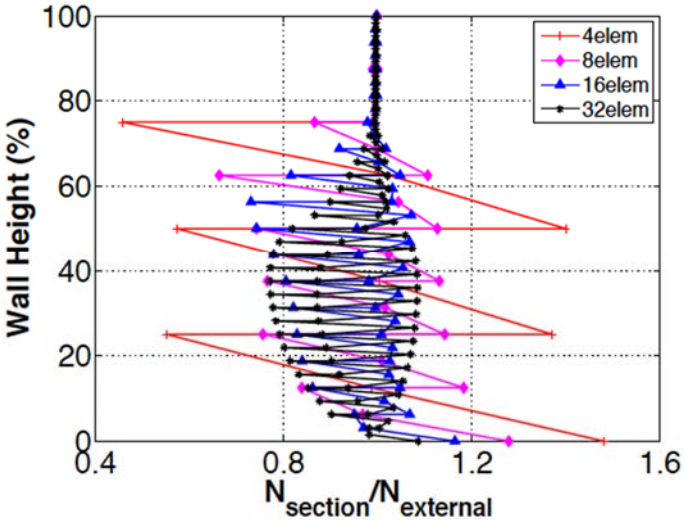

Figure 8: Normalized Axial Load (N) Ratio as Function of Wall Height

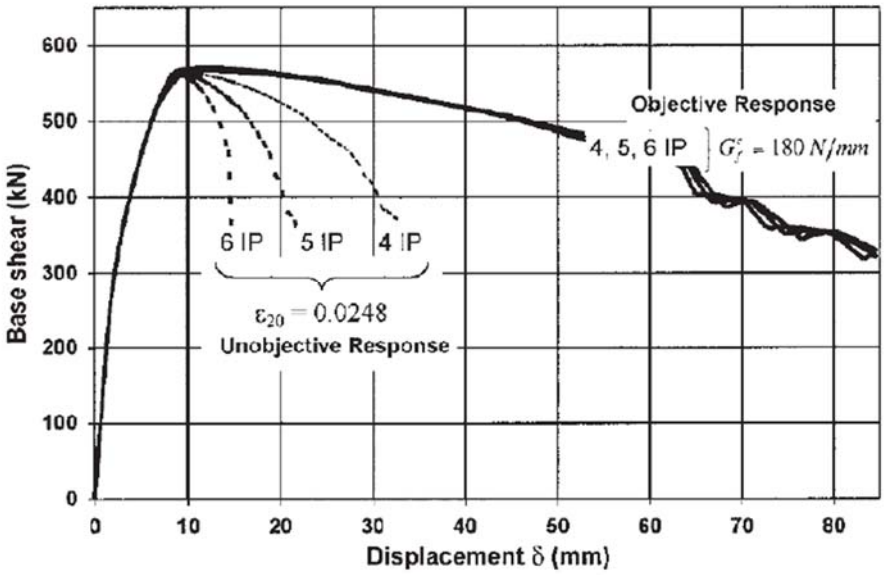

Figure 9: Objective vs. Non-objective Response (Coleman and Spacone 2001)

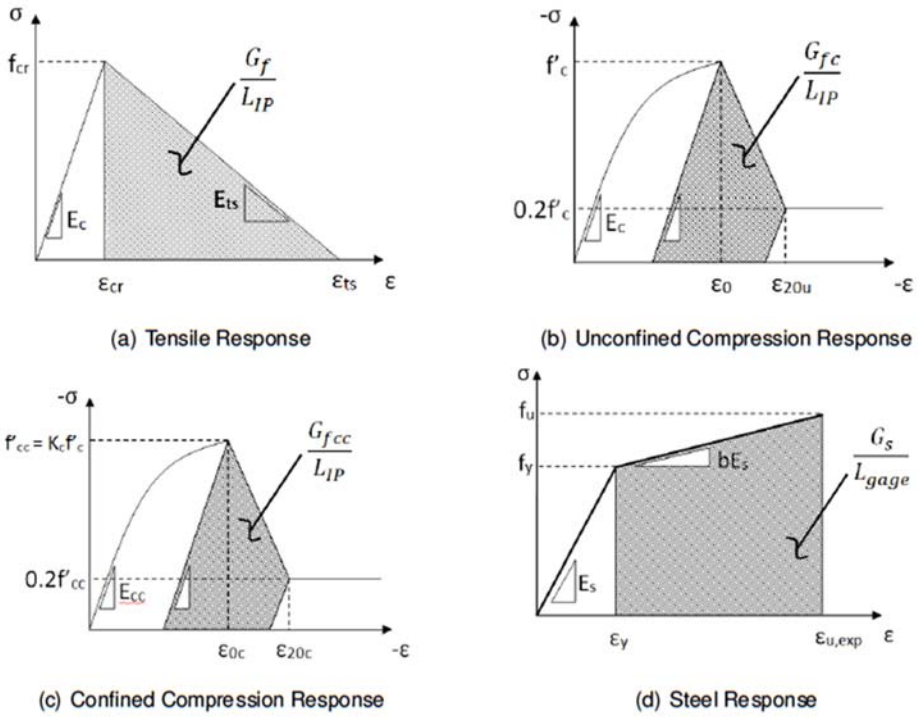

Figure 10: Regularized Material Constitutive Models

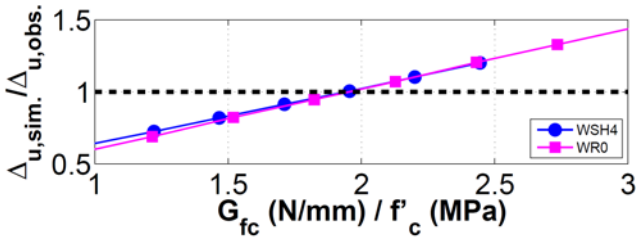

Figure 11: Unconfined Concrete Crushing Energy

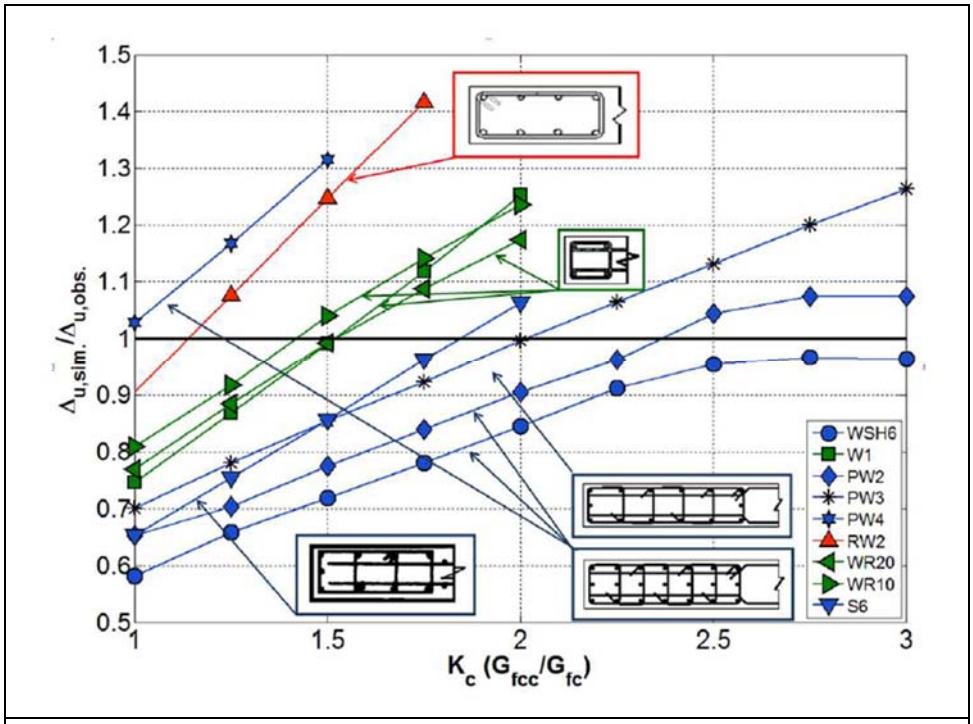

Figure 12: Evaluation of Energy Coefficient (K_c) for Confinement Concrete

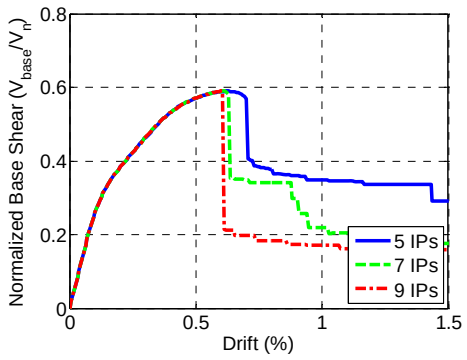

(a) WSH4, Basic Model, No Material Regularization

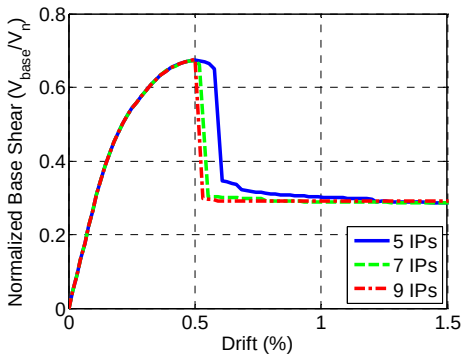

(b) WR0, Basic Model, No Material Regularization

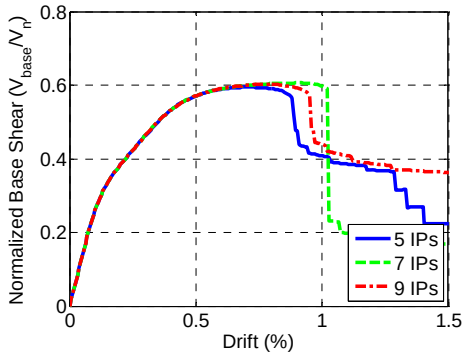

(c) WSH4, Concrete Material Regularization

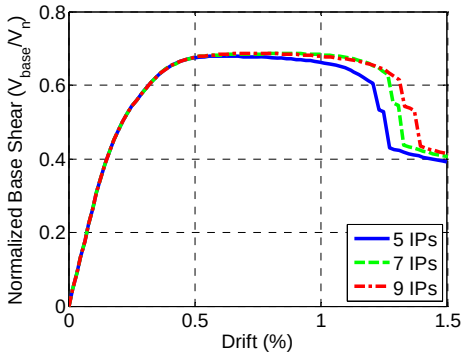

(d) WR0, Concrete Material Regularization

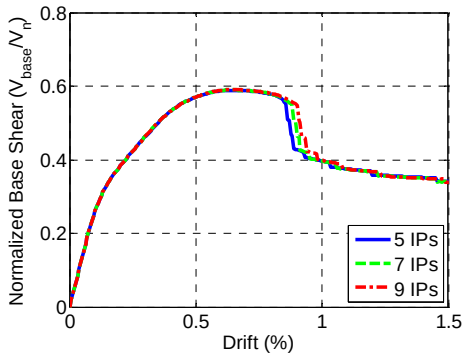

(e) WSH4, Regularized Model, Concrete and Steel Material Regularization

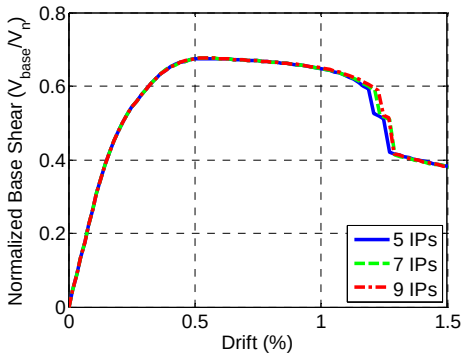

(g) WR0, Regularized Model, Concrete and Steel Material Regularization

Figure 13: Comparison of Two Specimens Simulated using (a) Basic Constitutive Models, (b) Concrete Regularization Only and (c) Steel and Concrete Regularization

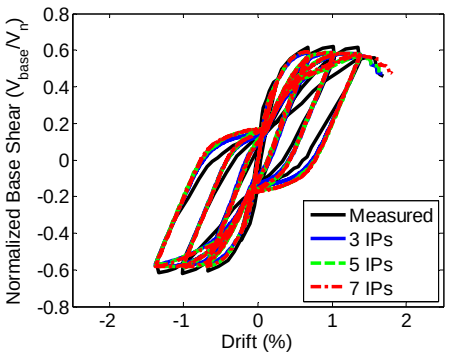

(a) WSH4, CB Failure, low shear stress demand

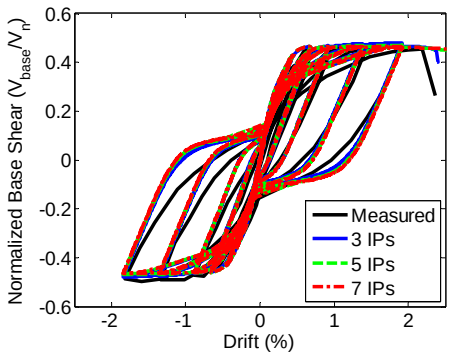

(b) WSH1, R Failure

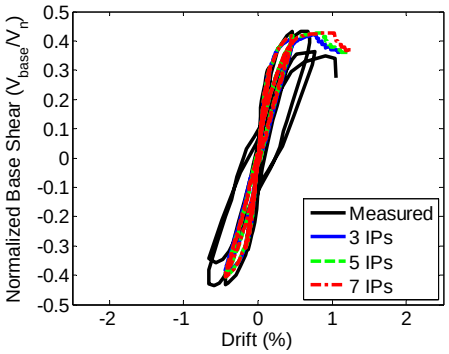

(c) RW1, BR Failure

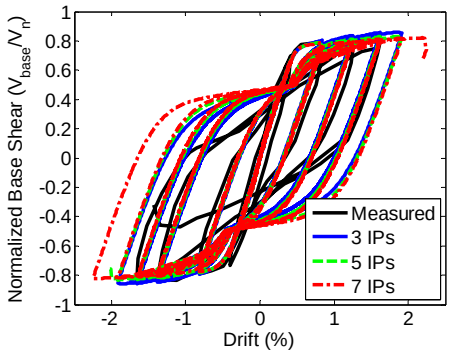

(d) S5, CB Failure, high shear stress demand

Figure 14: Comparison of Regularized Model and Measured Response for Selected Specimens

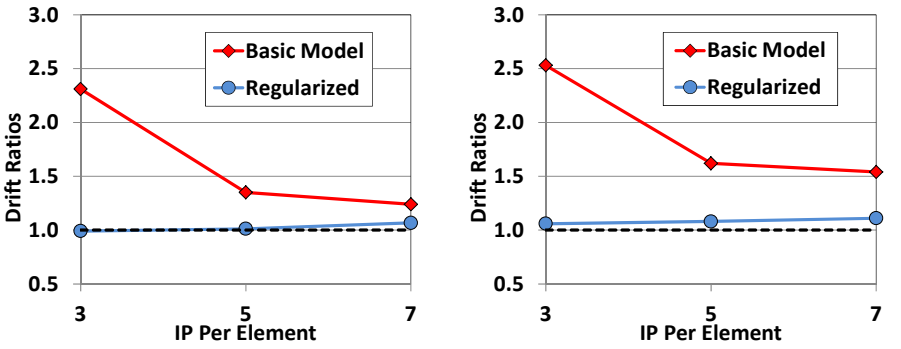

(a) F-CB Specimens (Force-Based) (b) F-BR Specimens (Force-Based)

Figure 15: Comparison of Median Drift Ratios for Both Modeling Approaches

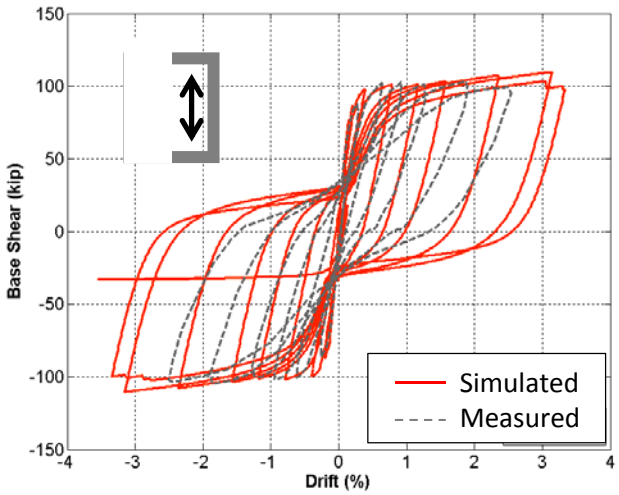

(a) ±X Loading TUA (Beyer et al. 2011)

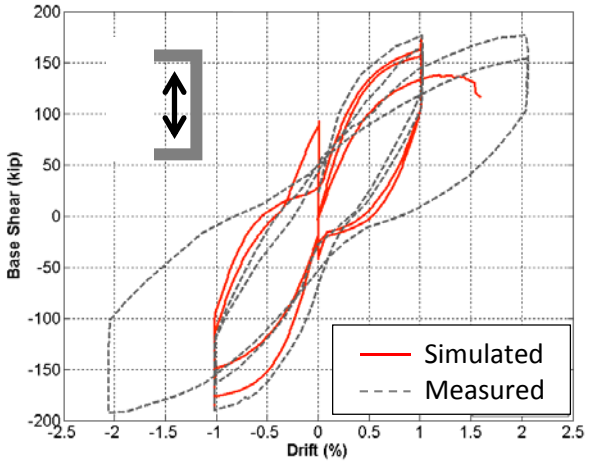

(b) ±X Loading W3 (Ile and Reynouard 2005)

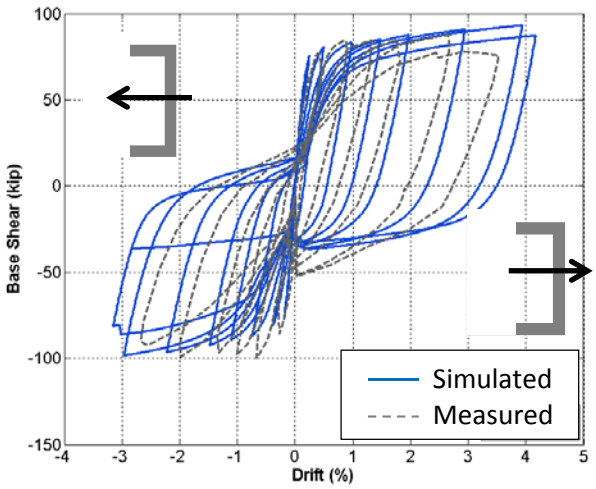

(c) ±Z Loading TUA (Beyer et al. 2011)

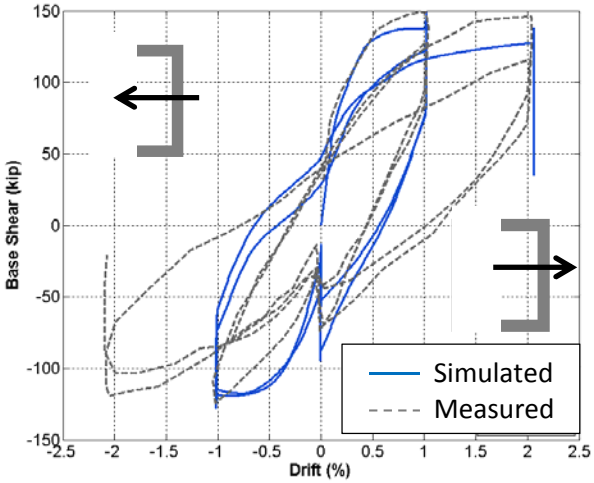

(b) ±Z Loading W3 (Ile and Reynouard 2005)

Figure 16: Simulated and Measured Response Histories for C-Shaped Walls

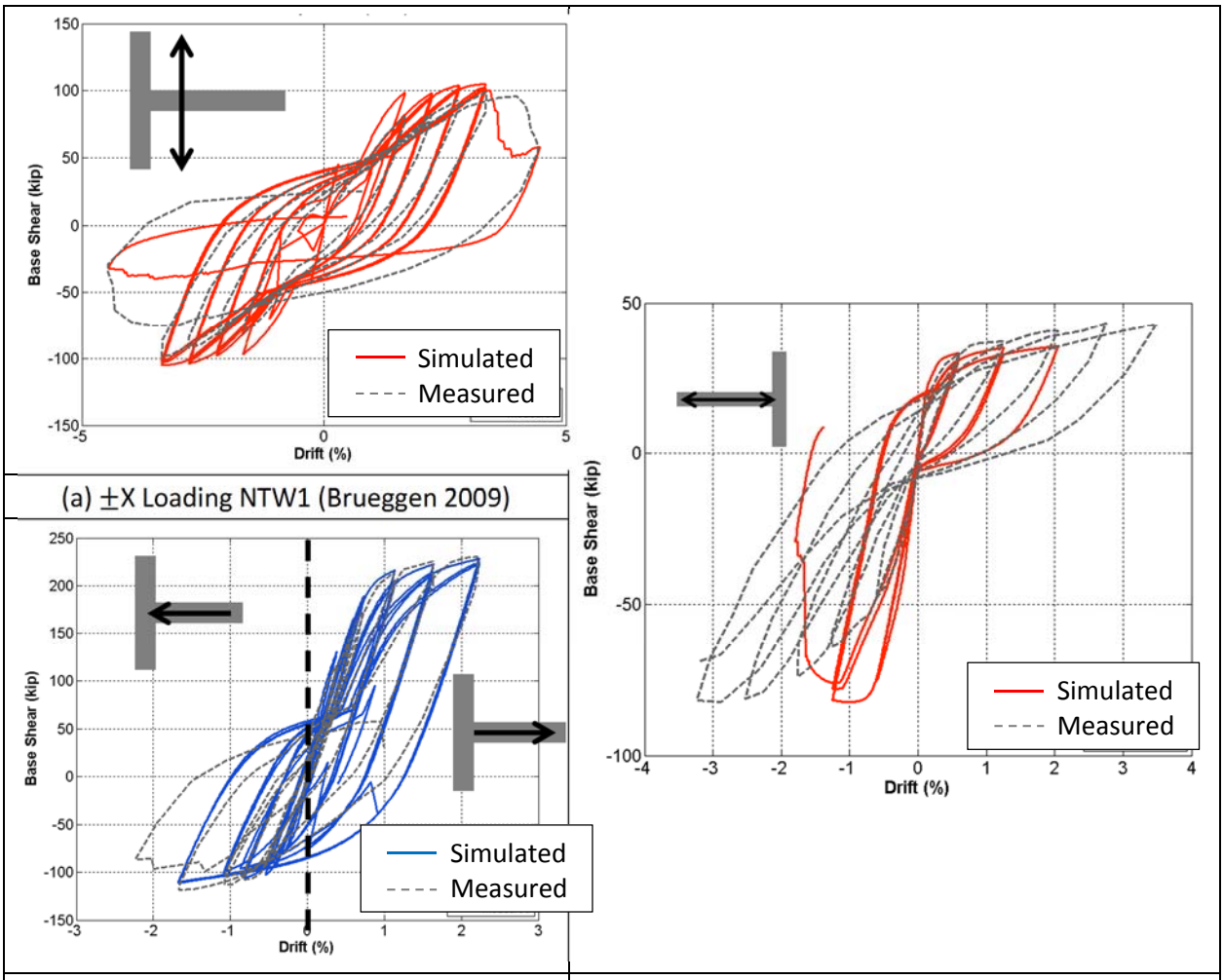

(a) ±X Loading NTW1 (Brueggen 2009)

(c) ±Z Loading NTW1 (Brueggen 2009)

(b) ±Z Loading TW2 (Thomsen and Wallace 2004)

Figure 17: Simulated and Measured Response Histories for T-Shaped Walls